MULTIHARMONIC ALGORITHMS FOR CONTRAST-ENHANCED ULTRASOUND

VANJA NIKOLIƆ AND TERESA RAUSCHER‡

ABSTRACT. Harmonic generation plays a crucial role in contrast-enhanced ultrasound, both for imaging and therapeutic applications. However, accurately capturing these nonlinear effects is computationally very demanding when using traditional time-domain approaches. To address this issue, in this work, we develop algorithms based on a time discretization that uses a multiharmonic Ansatz applied to a model that couples the Westervelt equation for acoustic pressure with a volume-based approximation of the Rayleigh–Plesset equation for the dynamics of microbubble contrast agents. We first rigorously establish the existence of time-periodic solutions for this Westervelt-ODE system. We then derive a multiharmonic representation of the system under time-periodic excitation and develop iterative algorithms that rely on the successive computation of higher harmonics under the assumption of real-valued or complex solution fields. In the real-valued setting, we characterize the approximation error in terms of the number of harmonics and a contribution owing to the fixed-point iteration. Finally, we investigate these algorithms numerically and illustrate how the number of harmonics and presence of microbubbles influence the propagation of acoustic waves.

1. Introduction

Contrast-enhanced ultrasound has become an important tool in biomedical applications, with gas-filled microbubbles being used to improve both diagnostic and therapeutic procedures. While ultrasound itself is inherently nonlinear, leading to the generation of higher harmonics in the frequency domain, these nonlinearities are further amplified by microbubble contrast agents, which exhibit highly nonlinear behavior themselves when exposed to ultrasound waves. This delicate back-and-forth interaction is beneficial for improving resolution in imaging but also for enhancing therapeutic treatments, such as targeted drug delivery; see, for example, [12, 17, 33] for details. With the rise in the number of applications of contrast-enhanced ultrasound, accurate modeling and efficient simulation in this context have also become prominent research topics; see, e.g., [6, 10, 27, 36], and the references given therein.

The present work builds upon [30], where time-domain mathematical models for ultrasound contrast imaging with microbubbles based on a nonlinear acoustic wave equation coupled to a Rayleigh-Plesset-type ODE have been derived and investigated in terms of local well-posedness and numerical simulations. As noted in [30], a big computational challenge when simulating such systems stems from different time scales on which the

²⁰²⁰ Mathematics Subject Classification. 35L05, 35L72, 34A34, 35J05.

Key words and phrases. nonlinear acoustics, contrast-enhanced ultrasound, microbubbles, multiharmonic expansions, Westervelt's equation, Helmholtz equation, iterative algorithms.

 $^{^\}dagger Department$ of Mathematics, Radboud University, Heyendaalseweg 135, 6525 AJ Nijmegen, The Netherlands (vanja.nikolic@ru.nl).

[‡]Department of Mathematics, Alpen-Adria-Universität Klagenfurt, Universitätsstraße 65–67, A-9020 Klagenfurt, Austria (teresa.rauscher@aau.at).

wave equation and ODE (nonlinearly) evolve. As a result, straightforward numerical approaches for solving such systems demand using very small time steps. In this work, we approach this issue by considering a volume formulation (approximation) of the Rayleigh-Plesset ODE and developing multiharmonic algorithms for time-periodic solution fields, which offer a potentially more efficient modeling alternative by making use of harmonic expansions; see, e.g., [3, 4], where multiharmonic ideas have been explored for problems arising in electromagnetism and [20, 21, 31], where they have been developed for single-physics acoustic models. Instead of resolving every oscillation in the space-time domain, these methods decompose the field into a sum of harmonics, which can be obtained as solutions of suitable (in our case) Helmholtz problems and algebraic equations. These methods are thus especially promising for simulating large-scale or real-time ultrasound applications as the number of used harmonics could potentially be relatively low.

As the starting time-domain model of contrast-enhanced ultrasound we employ the following coupled nonlinear wave-ODE system:

(1.1)
$$\begin{cases} p_{tt} - c^2 \Delta p - b \Delta p_t = \eta(x) (p^2)_{tt} + c^2 \rho_0 n_0(x) v_{tt} + h(x, t) & \text{in } \Omega \times (0, T), \\ v_{tt} + \delta \omega_0 v_t + \omega_0^2 v = \zeta(x) v^2 + \xi(x) (2v v_{tt} + v_t^2) - \mu(x) p & \text{in } \Omega \times (0, T), \end{cases}$$

consisting of the damped Westervelt equation [37] for the acoustic pressure p = p(x,t), that is, fluctuations in the background pressure, and an ODE (pointwise in space) for the volume variation v = v(x,t) of microbubbles. The total microbubble volume is given by $V = v_0 + v$, where v_0 is the equilibrium volume. The system in (1.1) models the interaction of pressure waves with the dynamics of the bubbles.

In the Westervelt equation, c denotes the speed of sound in the medium, b the diffusivity of sound (that is, the term $-b\Delta p_t$ introduces strong damping), ρ_0 the mass density of the mixture at equilibrium, and the nonlinearity coefficient is given by $\eta = \frac{\beta_a}{\rho_0 c^2}$, where β_a is the nonlinearity parameter in the medium. The source of the pressure waves is provided in part through a contribution due to bubble oscillations, modeled by the term $c^2 \rho_0 n_0 v_{tt}$, where n_0 is the bubble number density at equilibrium, and by the source function h = h(x,t). We allow the coefficients η and n_0 to vary in space (that is, we assume that η , $n_0 \in L^{\infty}(\Omega)$), as this setting is relevant for imaging applications; see, e.g., [24].

The ODE in (1.1) captures nonlinear harmonic oscillations driven by the acoustic pressure via the term $-\mu p$. The coefficient $\delta = \frac{4\nu}{\omega_0 R_0^2}$ is the viscous damping coefficient and $\omega_0 = \sqrt{\frac{3\kappa P_0}{\rho_0 R_0^2}}$ the natural frequency, where R_0 is the bubble radius at equilibrium volume v_0 (that is, $v_0 = \frac{4\pi}{3}R_0^3$), κ the adiabatic exponent and P_0 the ambient pressure in the mixture (so that the total pressure is $P_0 + p$).

The coefficients appearing on the right-hand side of the ODE are given in terms of equilibrium values by $\mu = \frac{4\pi R_0}{\rho_0}$, $\zeta = \frac{(\kappa+1)\omega_0^2}{2v_0}$, and $\xi = \frac{1}{6v_0}$. In the upcoming analysis, we allow these three functions to be space-variable, and furthermore we ask for the smallness of $\|\mu\|_{L^{\infty}(\Omega)}$ as a way of controlling the strength of the source of microbubble oscillations; see Theorem (2.1) for details. This smallness condition can be seen as imposing a size restriction on the bubble equilibrium radius R_0 .

As stated in [16, Ch. 5], the ODE in (1.1) can be seen an approximation of the following

Rayleigh–Plesset equation:

$$\rho_0 \left[RR_{tt} + \frac{3}{2}R_t^2 \right] = p_b - 4\nu \frac{R_t}{R} - p,$$

where ν is the viscosity and p_b a constant pressure contribution, which can be derived using the relation $V=\frac{4\pi}{3}R^3$ and the adiabatic gas law $\frac{p_b}{P_0}=\left(\frac{v_0}{V}\right)^\kappa$. Reformulating the dynamics in terms of v instead of R removes singular terms and results in a more manageable nonlinear structure. Since pressure perturbations couple more directly to volume oscillations, the volume-based formulation is also better suited for harmonic expansions. In contrast, a harmonic expansion in terms of R is expected to lead to higher-order interactions that complicate the isolation of harmonic components due to the cubic dependence of volume on radius.

We equip (1.1) with absorbing-type boundary conditions of the following form:

$$\beta p_t + \gamma p + \nabla p \cdot \mathbf{n} = 0$$
 on $\partial \Omega \times (0, T)$, $\beta, \gamma > 0$,

and we are interested in time-periodic solutions that satisfy

$$p(0) = p(T),$$
 $p_t(0) = p_t(T)$ in Ω ,
 $v(0) = v(T),$ $v_t(0) = v_t(T)$ in Ω .

Although in the existence analysis we do not require the source h to be time periodic, for developing multiharmonic algorithms, we assume that h represents the second time derivative of a T-periodic function g; see Section 3 for details.

Main contributions. The overall purpose of the present work is to establish multiharmonic approximation approaches for time-domain systems in the form of (1.1), that is, systems that incorporate both nonlinear acoustic propagation and nonlinear microbuble oscillations. To approximate the problem we employ a cut-off Fourier series for the pressure and volume fields:

$$(1.2) p \approx p^N = \Re\left\{\sum_{m=0}^N \exp(\imath m\omega t) p_m^N(x)\right\}, v \approx v^N = \Re\left\{\sum_{m=0}^N \exp(\imath m\omega t) v_m^N(x)\right\},$$

with $\omega = \frac{2\pi}{T}$. In addition to rigorously considering the setting of real-valued pressure-volume fields, we also discuss multiharmonic algorithms derived from complex-valued fields (that is, from dropping the \Re operator in (1.2)). This approach is sometimes adopted in electromagnetism (see, e.g., [9, 38]) and it has been discussed in [20] for the de-coupled Westervelt equation. Here, it results in simplified algorithms, which can be, however, only formally investigated; see Section 5 for details. Toward reaching the overall goal of the work, our main contributions pertain to

- rigorously establishing the existence of time-periodic solutions for the Westervelt-ODE system in (1.1);
- deriving cutoff multiharmonic approximations of the system under time-periodic excitation for computing (p_m^N, v_m^N) ;
- developing and investigating linearized multiharmonic cut-off algorithms for computing (p_m^N, v_m^N) .

In particular, we characterize the error of linearized multiharmonic algorithms for realvalued field in terms of the number of harmonics and a contribution due to the fixed-point iteration; see Theorem 4.1. For convenience, an overview of algorithms investigated in this work is provided in Figure 1.

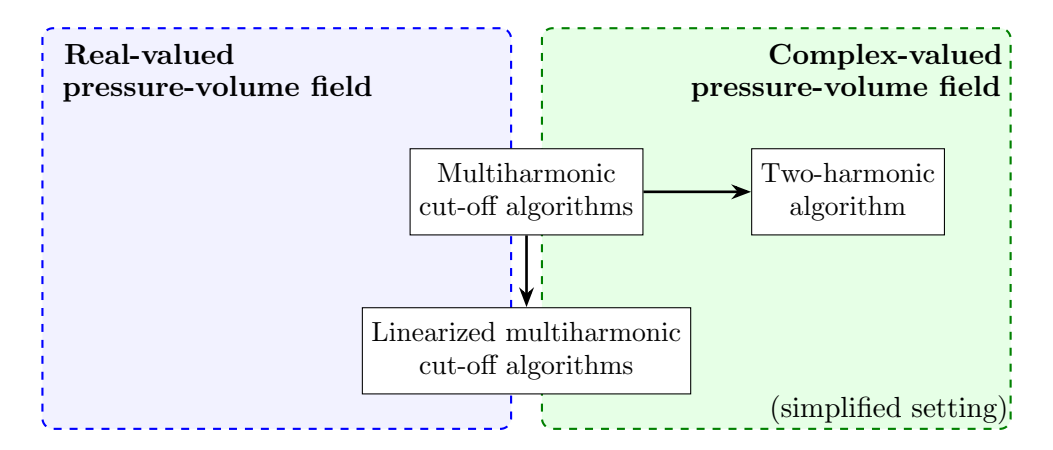


Figure 1. Overview of multiharmonic algorithms in this work.

Related work. Multiharmonic approaches of this type have been applied successfully to different problems arising in electromagnetism. In particular, a multiharmonic treatment of the quasi-stationery Maxwell problem has been developed and rigorously analyzed in [3]; numerical simulation aspects are discussed in [4]. In acoustics, an approach of second harmonic generation for a linearization of (1.1) with $\eta = 0$ and b = 0 in the wave equation has been formally derived in [16, Ch. 5]. In the setting of non-bubbly media, existence of periodic solutions of nonlinear acoustic models, including the Westervelt equation, has been investigated rigorously in [7, 8, 20–22, 31]. An iterative multiharmonic algorithm for the de-coupled Westervelt equation has been proposed and studied in [31].

Periodic solutions of Rayleigh–Plesset-type equations that do not incorporate modeling of the acoustic propagation have also been investigated in the literature; we refer to, for example, [15, 39] and [34, Ch. 9], and the references provided therein. We mention also that the mathematical literature on non-periodic models in nonlinear acoustics of non-bubbly media is quite rich; see, e.g., [1, 11, 19, 23] and the references provided therein.

Organization of the paper. The remaining of the exposition is organized as follows. In Section 2, we determine sufficient conditions for the well-posedness of the time-periodic boundary value problem for the Westervelt-ODE system (1.1). In Section 3, we derive a multiharmonic cut-off representation of the system and propose a linearization which results in a simplified setting for computing Fourier coefficients in (1.2). In Section 4, we characterize the error and prove the convergence of the proposed linearized multiharmonic scheme to the solution of the Westervelt-ODE system as the number of harmonics N tends to $+\infty$. The main theoretical result of the section is contained in Theorem 4.1. In Section 5, we discuss multiharmonic algorithms resulting from complex solutions fields. Finally, in Section 6, we investigate and compare the introduced algorithms.

2. Existence of time-periodic solutions

In this section, we establish the existence and uniqueness of periodic solutions for the coupled PDE-ODE system. More precisely, given T > 0 and a bounded domain $\Omega \subset \mathbb{R}^d$, where $d \in \{2,3\}$, we study the problem:

(2.1)
$$\begin{cases} p_{tt} - c^2 \Delta p - b \Delta p_t = \eta(x)(p^2)_{tt} + c^2 \rho_0 n_0(x) v_{tt} + h & \text{in } \Omega \times (0, T), \\ \beta p_t + \gamma p + \nabla p \cdot \boldsymbol{n} = 0 & \text{on } \partial \Omega \times (0, T), \\ p(0) = p(T), \ p_t(0) = p_t(T) & \text{in } \Omega, \\ v_{tt} + \delta \omega_0 v_t + \omega_0^2 v = \zeta(x) v^2 + \xi(x)(2v v_{tt} + v_t^2) - \mu(x) p & \text{in } \Omega \times (0, T), \\ v(0) = v(T), \ v_t(0) = v_t(T) & \text{in } \Omega. \end{cases}$$

The analysis will be based on successive approximations of the system, for which knowledge of linear time-periodic ODE and wave problems will be very helpful. We thus discuss those results next.

Notation. Below we use $x \lesssim y$ to denote $x \leq Cy$, where C > 0 is a generic constant. When writing norms in Bochner spaces, we omit the temporal domain (0,T). For example, $\|\cdot\|_{L^p(L^q(\Omega))}$ denotes the norm in $L^p(0,T;L^q(\Omega))$.

2.1. Auxiliary existence results for linear time-periodic problems. To set up the local well-posedness analysis of (2.1), we first state two separate results on the well-posedness of an ODE (describing damped oscillations with forcing) and a linear time-periodic wave problem.

Lemma 2.1. Let T > 0 and $f \in L^2(0,T;L^\infty(\Omega))$. Furthermore, let δ , $\omega_0 > 0$. Then, the periodic ODE problem

$$\begin{cases} v_{tt} + \delta\omega_0 v_t + \omega_0^2 v = f & a.e. \text{ in } \Omega \times (0, T), \\ v(0) = v(T), \ v_t(0) = v_t(T) & a.e. \text{ in } \Omega, \end{cases}$$

has a unique solution

$$v \in \mathcal{X}_v = \{v \in H^2(0, T; L^{\infty}(\Omega)) : v(0) = v(T), v_t(0) = v_t(T) \text{ a.e.}\}$$

that satisfies

$$||v||_{\mathcal{X}_v} := ||v||_{L^{\infty}(L^{\infty}(\Omega))} + ||v_t||_{L^{\infty}(L^{\infty}(\Omega))} + ||v_{tt}||_{L^2(L^{\infty}(\Omega))} \lesssim ||f||_{L^2(L^{\infty}(\Omega))}.$$

Proof. The existence and uniqueness can be established using Floquet theory (see, for example [32] and [14, Ch. 3]) as the only solution of the homogeneous problem is zero due to the fact that $\delta\omega_0 > 0$. The details are provided in Appendix A.

Proposition 2.1 (see [31, Theorem 2.1]). Let T > 0, $\Omega \subset \mathbb{R}^d$, where $d \in \{2,3\}$, be a bounded domain with $C^{1,1}$ boundary, and $\beta, \gamma > 0$, c, b > 0. Let $h \in L^2(0,T;L^2(\Omega))$. Then there exists a unique (weak) solution

$$p \in \mathcal{X}_p = \left\{ p \in H^2(0,T;L^2(\Omega)) \cap H^1(0,T;H^{3/2}(\Omega)) \cap L^2(0,T;H^2(\Omega)) : \\ ||\nabla p \cdot \mathbf{n}||_{H^1(L^2(\partial\Omega))} < \infty, \ ||\Delta p_t||_{L^2(L^2(\Omega))} < \infty, \ p(0) = p(T), \ p_t(0) = p_t(T) \ a.e. \right\}$$

of the time-periodic boundary-value problem

(2.2)
$$\begin{cases} p_{tt} - c^2 \Delta p - b \Delta p_t = h & in \ \Omega \times (0, T), \\ \beta p_t + \gamma p + \nabla p \cdot \boldsymbol{n} = 0 & on \ \partial \Omega \times (0, T), \\ p(0) = p(T), \ p_t(0) = p_t(T) & in \ \Omega. \end{cases}$$

The solution satisfies

$$||p||_{\mathcal{X}_p} := ||p||_{L^2(H^2(\Omega))} + ||p_t||_{L^2(H^{3/2}(\Omega))} + ||p_{tt}||_{L^2(L^2(\Omega))} + ||\Delta p_t||_{L^2(L^2(\Omega))} + ||\nabla p \cdot \mathbf{n}||_{H^1(L^2(\partial\Omega))}$$

$$\leq C(b, \gamma, c, \beta, T, \Omega) ||h||_{L^2(0,T;L^2(\Omega))},$$

for some constant $C = C(b, \gamma, c, \beta, T, \Omega) > 0$, independent of h.

We note that having $\gamma > 0$ in (2.2) is crucial for uniqueness. Furthermore, having strong damping (that is, $-b\Delta p_t$ with b>0) in the wave equation contributes to its parabolic-like character, and is heavily exploited in the proof of the above statement. We also note that the functions f and h do not have to be time periodic for the well-posedness results in this section, although we will make that assumption on the acoustic source in Section 3 to develop (iterative) multiharmonic algorithms.

2.2. Analysis of the Westervelt-ODE system. Equipped with the previous results on linear problems, we are now ready to prove the well-posedness of the coupled pressure-volume problem. To state it, we introduce

$$\mathbb{B}_{r_p,r_v} = \left\{ (p,v) \in \mathcal{X}_p \times \mathcal{X}_v : \|p\|_{\mathcal{X}_p} \le r_p, \|v\|_{\mathcal{X}_v} \le r_v \right\},\,$$

where $r_p > 0$ and $r_v > 0$ will be set as small enough in the course of the proof below. The proof will have constructive nature using successive approximations, and we will later adopt the same linearization approach in Section 3.2 when setting up multiharmonic iterations.

Theorem 2.1. Let T > 0, $\Omega \subseteq \mathbb{R}^d$, $d \in \{2,3\}$, be open, bounded, connected, with $C^{1,1}$ boundary, β , γ , c, b, δ , $\omega_0 > 0$ and η , μ , ζ , ξ , $n_0 \in L^{\infty}(\Omega)$, $h \in L^2(0,T;L^2(\Omega))$. Then there exist $\delta_p > 0$ and $\delta_v > 0$, such that if

$$||h||_{L^2(0,T;L^2(\Omega))} \le \delta_p \quad and \quad ||\mu||_{L^\infty(\Omega)} \le \delta_v,$$

then there exist radii $r_p > 0$ and $r_v > 0$, such that problem (2.1) has a unique solution $(p, v) \in \mathbb{B}_{r_p, r_v}$.

Proof. As announced, the proof follows by constructing the solutions using successive approximations.

Let $r_p, r_v > 0$. We take $(p^{(0)}, v^{(0)}) \in \mathbb{B}_{r_p, r_v}$ and set up successive approximations using the system given by

$$(2.3a) \begin{cases} p_{tt}^{(N)} - c^2 \Delta p^{(N)} - b \Delta p_t^{(N)} = \eta((p^{(N-1)})^2)_{tt} + c^2 \rho_0 n_0 v^{(N)} + h & \text{in } \Omega \times (0, T), \\ \beta p_t^{(N)} + \gamma p^{(N)} + \nabla p^{(N)} \cdot \boldsymbol{n} = 0 & \text{on } \partial \Omega \times (0, T), \\ p^{(N)}(0) = p^{(N)}(T), \ p_t^{(N)}(0) = p_t^{(N)}(T) & \text{in } \Omega, \end{cases}$$

and

(2.3b)
$$\begin{cases} v_{tt}^{(N)} + \delta\omega_0 v_t^{(N)} + \omega_0^2 v^{(N)} \\ = -\mu p^{(N-1)} + \zeta (v^{(N-1)})^2 - \xi \left(2v^{(N-1)} v_{tt}^{(N-1)} + (v_t^{(N-1)})^2 \right) & \text{in } \Omega \times (0, T), \\ v^{(N)}(0) = v^{(N)}(T), \ v_t^{(N)}(0) = v_t^{(N)}(T) & \text{in } \Omega. \end{cases}$$

• Let N=1. Note that we can first solve (2.3b) and use its solution as the input for solving (2.3a). By Lemma 2.1, we have a unique $v^{(1)} \in \mathcal{X}_v$ that solves (2.3b), such that

$$||v^{(1)}||_{\mathcal{X}_v} \le C(||\mu||_{L^{\infty}(\Omega)}||p^{(0)}||_{L^2(L^{\infty}(\Omega))} + (||\zeta||_{L^{\infty}(\Omega)} + ||\xi||_{L^{\infty}(\Omega)})||v^{(0)}||_{\mathcal{X}_v}^2).$$

From here, we find that

$$||v^{(1)}||_{\mathcal{X}_v} \le C(||\mu||_{L^{\infty}(\Omega)}r_p + (||\zeta||_{L^{\infty}(\Omega)} + ||\xi||_{L^{\infty}(\Omega)})r_v^2)$$

and we can conclude that $||v^{(1)}||_{\mathcal{X}_v} \leq r_v$ provided $||\mu||_{L^{\infty}(\Omega)}$ is small enough by possibly reducing r_v . By Proposition 2.1, the linear problem in(2.3a) for N=1 has a unique solution $p^{(1)} \in \mathcal{X}_p$, such that

$$||p^{(1)}||_{\mathcal{X}_p} \leq C||-\eta((p^0)^2)_{tt} - c^2\rho_0 n_0 v_{tt}^1 + h||_{L^2(L^2(\Omega))}$$

$$\leq C\left(||\eta||_{L^{\infty}(\Omega)}||p^0||_{\mathcal{X}_p}^2 + ||n_0||_{L^{\infty}(\Omega)}||v^{(1)}||_{\mathcal{X}_v} + ||h||_{L^2(L^2(\Omega))}\right).$$

By using the fact that $||v^{(1)}||_{\mathcal{X}_v} \leq r_v$, we obtain

$$||p^{(1)}||_{\mathcal{X}_p} \le C \left(||\eta||_{L^{\infty}(\Omega)} r_p^2 + ||n_0||_{L^{\infty}(\Omega)} r_v + ||h||_{L^2(L^2(\Omega))} \right).$$

From here, we can conclude that $||p^{(1)}||_{\mathcal{X}_p} \leq r_p$ for small enough $||h||_{L^2(L^2(\Omega))}$ by possibly reducing r_p and r_v .

• Let now $(p^{(N-1)}, v^{(N-1)}) \in \mathbb{B}_{r_p, r_v}$. By Lemma 2.1, we have

$$||v^{(N)}||_{\mathcal{X}_v} \le C(||\mu||_{L^{\infty}(\Omega)}||p^{(N-1)}||_{L^2(L^{\infty}(\Omega))} + ||v^{(N-1)}||_{\mathcal{X}_v}^2)$$

and by Proposition 2.1, the linear problem in (2.3a) with periodic time conditions has a unique solution $p^{(N)} \in \mathcal{X}_p$, such that

$$||p^{(N)}||_{\mathcal{X}_p} \le C||-\eta((p^{(N-1)})^2)_{tt} - c^2\rho_0 n_0 v_{tt}^{(N)} + h||_{L^2(L^2(\Omega))}$$

$$\le C\left(||\eta||_{L^{\infty}(\Omega)}||p^{(N-1)}||_{\mathcal{X}_p}^2 + ||n_0||_{L^{\infty}(\Omega)}||v^{(N)}||_{\mathcal{X}_v} + ||h||_{L^2(L^2(\Omega))}\right).$$

By then proceeding analogously to the case N=1, we obtain

$$||p^{(N)}||_{\mathcal{X}_n} \le r_p, \quad ||v^{(N)}||_{\mathcal{X}_v} \le r_v,$$

provided $\|\mu\|_{L^{\infty}(\Omega)}$ and $\|h\|_{L^{2}(L^{2}(\Omega))}$ are small enough. We thus conclude that for small enough $\|h\|_{L^{2}(L^{2}(\Omega))}$ and $\|\mu\|_{L^{\infty}(\Omega)}$, there exist $r_{p} > 0$ and $r_{v} > 0$, such that if $(p^{(0)}, v^{(0)}) \in \mathbb{B}_{r_{p}, r_{v}}$, then for each $N \geq 1$, problem (2.3) has a unique solution $(p^{(N)}, v^{(N)}) \in \mathbb{B}_{r_{p}, r_{v}}$.

• We next wish to show that $\{(p^{(N)}, v^{(N)})\}_{N\geq 1}$ is a Cauchy sequence in $\mathcal{X}_p \times \mathcal{X}_v$. We

note that for $N_1, N_2 \in \mathbb{N}$, the difference $(\overline{p}, \overline{v}) = (p^{(N_1)} - p^{(N_2)}, v^{(N_1)} - v^{(N_2)})$ solves

$$\begin{cases} \overline{p}_{tt} - c^2 \Delta \overline{p} - b \Delta \overline{p}_t \\ = -\eta ((p^{(N_1 - 1)} - p^{(N_2 - 1)})(p^{(N_1 - 1)} + p^{(N_2 - 1)}))_{tt} - c^2 \rho_0 n_0 (v_{tt}^{(N_1)} - v_{tt}^{(N_2)}) & \text{in } \Omega \times (0, T), \\ \beta \overline{p}_t + \gamma \overline{p} + \nabla \overline{p} \cdot \boldsymbol{n} = 0 & \text{on } \partial \Omega \times (0, T), \end{cases}$$

and

$$\begin{split} \overline{v}_{tt} + \delta\omega_0 \overline{v}_t + \omega_0^2 \overline{v} \\ &= -\mu(p^{(N_1-1)} - p^{(N_2-1)}) + \zeta(v^{(N_1-1)} - v^{(N_2-1)})(v^{(N_1-1)} + v^{(N_2-1)}) \\ &\qquad - \xi \left(2(v^{(N_1-1)} - v^{(N_2-1)})v_{tt}^{(N_1-1)} \right. \\ &\qquad + v^{(N_2-1)}(v_{tt}^{(N_1-1)} - v_{tt}^{(N_2-1)}) + (v_t^{(N_1-1)} - v_t^{(N_2-1)})(v_t^{(N_1-1)} + v_t^{(N_2-1)})). \end{split}$$

From here, similarly to before, using Proposition 2.1 and Lemma 2.1, we obtain

$$||p^{(N_1)} - p^{(N_2)}||_{\mathcal{X}_p} \le C||\eta||_{L^{\infty}(\Omega)} r_p ||p^{(N_1 - 1)} - p^{(N_2 - 1)}||_{\mathcal{X}_p} + C||n_0||_{L^{\infty}(\Omega)} ||v^{(N_1)} - v^{(N_2)}||_{\mathcal{X}_v}$$
 and

$$(2.5) ||v^{(N_1)} - v^{(N_2)}||_{\mathcal{X}_v} \le C||\mu||_{L^{\infty}(\Omega)}||p^{(N_1 - 1)} - p^{(N_2 - 1)}||_{\mathcal{X}_p} + Cr_v||v^{(N_1 - 1)} - v^{(N_2 - 1)}||_{\mathcal{X}_v}.$$

By plugging the second inequality into the first one, we obtain

$$||p^{(N_1)} - p^{(N_2)}||_{\mathcal{X}_p}$$

$$\leq C(||\eta||_{L^{\infty}(\Omega)}r_p + ||n_0||_{L^{\infty}(\Omega)}||\mu||_{L^{\infty}(\Omega)})||p^{(N_1-1)} - p^{(N_2-1)}||_{\mathcal{X}_p}$$

$$+ C||n_0||_{L^{\infty}(\Omega)}r_v||v^{(N_1-1)} - v^{(N_2-1)}||_{\mathcal{X}_v}.$$

Adding (2.5) and (2.6) then yields

$$||p^{(N_1)} - p^{(N_2)}||_{\mathcal{X}_p} + ||v^{(N_1)} - v^{(N_2)}||_{\mathcal{X}_v}$$

$$\leq C(||\eta||_{L^{\infty}(\Omega)}r_p + (||n_0||_{L^{\infty}(\Omega)} + 1)||\mu||_{L^{\infty}(\Omega)})||p^{(N_1-1)} - p^{(N_2-1)}||_{\mathcal{X}_p}$$

$$+ C(||n_0||_{L^{\infty}(\Omega)} + 1)r_v||v^{(N_1-1)} - v^{(N_2-1)}||_{\mathcal{X}_v}.$$

We can exploit the smallness of r_p , $\|\mu\|_{L^{\infty}(\Omega)}$, and r_v and use this inequality to conclude that $\{(p^{(N)}, v^{(N)})\}_{N\geq 1}$ is a Cauchy sequence. Thus, there exists (p, v) such that $\{(p^{(N)}, v^{(N)})\}_{N\geq 1}$ converges to it in $\mathcal{X}_p \times \mathcal{X}_v$. Passing to the limit in (2.3) proves that (p, v) solves the pressure-volume problem.

• Finally, to show that such a constructed solution is unique, we take

$$(p^{<1>}, v^{<1>}), (p^{<2>}, v^{<2>}) \in \mathbb{B}_{r_p, r_v},$$

and note that the difference $(\overline{p}, \overline{v}) = (p^{<1>} - p^{<2>}, v^{<1>} - v^{<2>})$ solves

$$\begin{cases} \overline{p}_{tt} - c^2 \Delta \overline{p} - b \Delta \overline{p}_t = -\eta (\overline{p}(p^{<1>} + p^{<2>}))_{tt} - c^2 \rho_0 n_0 \overline{v}_{tt} & \text{in } \Omega \times (0, T), \\ \beta \overline{p}_t + \gamma \overline{p} + \nabla \overline{p} \cdot \boldsymbol{n} = 0 & \text{on } \partial \Omega \times (0, T), \end{cases}$$

and

$$\overline{v}_{tt} + \delta\omega_0\overline{v}_t + \omega_0^2\overline{v} = -\mu\overline{p} + \zeta\overline{v}\left(v^{<1>} + v^{<2>}\right) - \xi\left(2(\overline{v}v_{tt}^{<1>} + v^{<2>}\overline{v}_{tt}) + \overline{v}_t(v_t^{<1>} + v_2^{<2>})\right).$$

We obtain similarly to before

(2.7a)
$$\|\overline{p}\|_{\mathcal{X}_p} \lesssim \|\eta\|_{L^{\infty}(\Omega)} r_p \|\overline{p}\|_{\mathcal{X}_p} + \|n_0\|_{L^{\infty}(\Omega)} \|\overline{v}\|_{\mathcal{X}_v}$$

and

(2.7b)
$$\|\overline{v}\|_{\mathcal{X}_v} \lesssim \|\mu\|_{L^{\infty}(\Omega)} \|\overline{p}\|_{\mathcal{X}_p} + r_v \|\overline{v}\|_{\mathcal{X}_v}.$$

From here, by adding λ ·(2.7a) and (2.7b) we have for $\lambda > 0$

$$\lambda \|\overline{p}\|_{\mathcal{X}_p} + \|\overline{v}\|_{\mathcal{X}_v} \lesssim (\lambda \|\eta\|_{L^{\infty}(\Omega)} r_p + \|\mu\|_{L^{\infty}(\Omega)}) \|\overline{p}\|_{\mathcal{X}_p} + (\lambda \|n_0\|_{L^{\infty}(\Omega)} + r_v) \|\overline{v}\|_{\mathcal{X}_v}.$$

If C>0 is the hidden constant above, choosing r_p , r_v , $\|\mu\|_{L^{\infty}(\Omega)}$, and λ so that

$$C(r_v + \lambda || n_0 ||_{L^{\infty}(\Omega)}) < 1, \qquad C(||\mu||_{L^{\infty}(\Omega)} + \lambda ||\eta||_{L^{\infty}(\Omega)} r_p) < \lambda,$$

allows us to conclude that $\|\overline{p}\|_{\mathcal{X}_p} = \|\overline{v}\|_{\mathcal{X}_v} = 0$. This step completes the proof.

We note that the small-data setting of Theorem 2.1 effectively forces the nonlinear ODE to retain the damped harmonic oscillator structure with T-periodic coefficients. Indeed, under the assumptions of Theorem 2.1, for r_v small enough, so that

$$\max \left\{ 2\|\xi\|_{L^{\infty}(\Omega)}, \frac{1}{\delta\omega_0} \|\xi\|_{L^{\infty}(\Omega)}, \frac{1}{\omega_0^2} \|\zeta\|_{L^{\infty}(\Omega)} \right\} \cdot r_v < 1,$$

we can rewrite the ODE in the following form:

$$v_{tt} + \frac{\delta\omega_0 - \xi v_t}{1 - 2\xi v} v_t + \frac{\omega_0^2 - \zeta v}{1 - 2\xi v} v = -\frac{\mu}{1 - 2\xi v} p.$$

Setting $\ell = \frac{\delta\omega_0 - \xi v_t}{1 - 2\xi v} > 0$, $q = \frac{\omega_0^2 - \zeta v}{1 - 2\xi v} > 0$, and $f = -\frac{\mu}{1 - 2\xi v}p$, we see that the volume fluctuation v can be represented as the solution of a second-order ODE (pointwise a.e. in space) with positive T-periodic coefficients and a T-periodic right-hand side, namely

$$v_{tt} + \ell(t)v_t + q(t)v = f(t),$$

where $\ell(0) = \ell(T)$, q(0) = q(T), f(0) = f(T).

3. Time discretization via a multiharmonic Ansatz for real fields

In this section, we discuss the time discretization of the system by using a multiharmonic Ansatz, in the general spirit of [20]. We focus on a special case of having T-periodic acoustic excitation. That is, we assume that the acoustic source term has the form $h = g_{tt}$, where the function g is given by

(3.1)
$$g(x,t) = \Re\left\{\sum_{m=0}^{M} \exp(im\omega t) h_m^M(x)\right\}, \quad \omega = \frac{2\pi}{T}, \quad h \in L^2(\Omega; \mathbb{C}).$$

Under the assumptions of Theorem 2.1, a unique time-periodic solution (p, v) of the system given in (2.1) exists. For numerical approximations, we thus employ the following multiharmonic Ansatz:

(3.2)
$$u^{N}(x,t) = \frac{1}{2} \sum_{m=0}^{N} \left(\exp(im\omega t) u_{m}^{N}(x) + \exp(-im\omega t) \overline{u_{m}^{N}(x)} \right)$$
$$= \Re \left\{ \sum_{m=0}^{N} \exp(im\omega t) u_{m}^{N}(x) \right\}.$$

Alternatively, the multiharmonic Ansatz can be written in a more standard Fourier series form:

$$u^{N}(x,t) = \sum_{m=0}^{N} \left[u_{m}^{c}(x) \cos(k\omega t) + u_{m}^{s}(x) \sin(m\omega t) \right]$$

with $u_m^N(x) = u_m^c(x) - \imath u_m^s(x)$. We then look for the approximate pressure-volume field $(p^N, v^N) \in X_N \times X_N$, with

$$X_N = \left\{ \Re \left\{ \sum_{m=0}^N \exp(\imath m \omega t) u_m^N(x) \right\} \, : \, u_m^N \in H^2(\Omega; \mathbb{C}) \right\},$$

where the coefficients (p_m^N, v_m^N) in the expansion are determined from the following system:

$$\begin{cases}
p_{tt}^{N} - c^{2}\Delta p^{N} - b\Delta p_{t}^{N} \\
= \eta \operatorname{Proj}_{X_{N}} \left[((p^{N})^{2})_{tt} \right] + c^{2}\rho_{0}n_{0}v^{N} + \operatorname{Proj}_{X_{N}}h & \text{in } \Omega \times (0, T), \\
\beta p_{t}^{N} + \gamma p^{N} + \nabla p^{N} \cdot \boldsymbol{n} = 0 & \text{on } \partial\Omega \times (0, T), \\
v_{tt}^{N} + \delta\omega_{0}v_{t}^{N} + \omega_{0}^{2}v^{N} \\
= -\mu p^{N} + \operatorname{Proj}_{X_{N}} \left[\zeta(v^{N})^{2} + \xi \left(2v^{N}v_{tt}^{N} + (v_{t}^{N})^{2} \right) \right] & \text{in } \Omega \times (0, T).
\end{cases}$$

We next wish to show that (3.3) can be equivalently rewritten as a system of Helmholtz problems and algebraic equations for computing (p_m^N, v_m^N) .

3.1. A multiharmonic cut-off algorithm. Below we skip writing the dependencies of Fourier coefficients on x for readability.

Proposition 3.1. Let the assumptions of Theorem 2.1 hold with the acoustic source term assumed to have the form $h = g_{tt}$, where g is given in (3.1). The problem in (3.3) yields the following coupled system for computing (p_m^N, v_m^N) for $N \ge 0$ and $0 \le m \le N$:

$$\begin{split} m &= 0: \begin{cases} (i) & p_0^N = 0, \\ (ii) & \omega_0^2 v_0^N = \zeta \left(v_0^N\right)^2 + \sum_{j=1}^N \left(\frac{\zeta}{2} - \frac{\xi}{2}\omega^2 j^2\right) \left|v_j^N\right|^2, \\ m &= 1: \begin{cases} (i) & -p_1^N - \frac{c^2 + \imath b\omega}{\omega^2} \Delta p_1^N + c^2 n_0 \rho_0 v_1^N = -h_1^N - \sum_{k=3:2}^{2N-1} \eta \overline{p_{\frac{N-1}{2}}^N} p_{\frac{k+1}{2}}^N, \\ (ii) & \left(-\omega^2 + \imath \delta \omega_0 \omega - \omega_0^2\right) v_1^N + \mu p_1^N \\ &= (\zeta - \xi \omega^2) v_0^N v_1^N + \sum_{k=1:2}^{2N-1} \left(\zeta - \xi \omega^2 \frac{k^2 + 3}{4}\right) \overline{v_{\frac{N-1}{2}}^N} v_{\frac{k+1}{2}}^N, \end{split}$$

$$m = \{2, \dots, N\} : \begin{cases} (i) & -p_m^N - \frac{c^2 + \imath mb\omega}{m^2\omega^2} \Delta p_m^N + c^2 \rho_0 n_0 v_m^N \\ & = -h_m^N - \eta \left(\sum_{l=1}^{m-1} p_l^N p_{m-l}^N - 2 \sum_{k=m+2:2}^{2N-m} \overline{p_{\frac{k-m}{2}}^N} p_{\frac{k+m}{2}}^N \right), \\ (ii) & \left(-\omega^2 + \imath \delta \omega_0 \omega + \omega_0^2 \right) v_m^N + \mu p_m^N, \\ & = \sum_{l=0}^m \left(\frac{\zeta}{2} - \frac{\xi \omega^2}{2} (m-l) (2m-l) \right) v_l^N v_{m-l}^N \\ & + \sum_{k=m:2}^{2N-m} \left(\zeta - \xi \omega^2 \frac{k^2 + 3m^2}{4} \right) \overline{v_{\frac{k-m}{2}}^N} v_{\frac{k+m}{2}}^N. \end{cases}$$

Additionally, each of the individual functions p_m^N for $m \in \{1, ..., N\}$ satisfies the following boundary conditions:

(3.4)
$$(i\omega m\beta + \gamma)p_m^N + \nabla p_m^N \cdot \mathbf{n} = 0 \quad on \ \partial\Omega.$$

Proof. We begin by considering the derivation of the multiharmonic algorithm for the Westervelt's equation and the ODE separately. For the PDE, one can follow the steps outlined in [20], where the de-coupled Westervelt equation is considered, by setting the right-hand side to $g = h + c^2 \rho_0 n_0 v$. Projections onto X_N of product terms appearing on the right-hand side of (3.3) can be expressed using [20, Lemma 3.1].

For the ODE in (3.3), the Ansatz given in (3.2), together with [20, Lemma 3.1], yields

$$0 = \Re \left\{ -\omega^2 \sum_{m=0}^{N} v_m^N m^2 \exp(im\omega t) + \delta \omega_0 i\omega \sum_{m=0}^{N} v_m^N m \exp(im\omega t) + \omega_0^2 \sum_{m=0}^{N} v_m^N \exp(im\omega t) + \mu \sum_{m=0}^{N} p_m^N \exp(im\omega t) - \frac{\zeta}{2} \left((v_0^N)^2 + \sum_{j=0}^{N} |v_j^N|^2 + \sum_{m=1}^{N} \left[\sum_{l=0}^{m} v_l^N v_{m-l}^N + 2 \sum_{k=m:2}^{2N-m} \overline{v_{\frac{k-m}{2}}^N} v_{\frac{k+m}{2}}^N \right] \exp(im\omega t) \right) + \xi \frac{\omega^2}{2} \left(\sum_{j=0}^{N} j^2 |v_j^N|^2 + \sum_{m=1}^{N} \left[\sum_{l=0}^{m} (m-l)(2m-l)v_l^N v_{m-l}^N + \sum_{k=m:2}^{2N-m} \frac{k^2 + 3m^2}{2} \overline{v_{\frac{k-m}{2}}^N} v_{\frac{k+m}{2}}^N \right] \exp(im\omega t) \right) \right\}.$$

From here, we have

$$\begin{split} 0 = &\Re\left\{\sum_{m=0}^{N}\left[\left(-\omega^{2}m^{2} + \delta\omega_{0}\imath\omega m + \omega_{0}^{2}\right)v_{m}^{N} + \mu p_{m}^{N}\right]\exp(\imath m\omega t) \right. \\ &\left. -\frac{\zeta}{2}(v_{0}^{N})^{2} + \sum_{j=0}^{N}\left(-\frac{\zeta}{2} + \xi\frac{\omega^{2}}{2}j^{2}\right)\left|v_{j}^{N}\right|^{2} + \sum_{m=1}^{N}\left[\sum_{l=0}^{m}\left(-\frac{\zeta}{2} + \xi\frac{\omega^{2}}{2}(m-l)(2m-l)\right)v_{l}^{N}v_{m-l}^{N} + \sum_{k=m:2}^{2N-m}\left(-\zeta + \xi\omega^{2}\frac{k^{2} + 3m^{2}}{4}\right)\overline{v_{\frac{k-m}{2}}^{N}}v_{\frac{k+m}{2}}^{N}\right]\exp(\imath m\omega t)\right\}. \end{split}$$

Combining our derivations above and using linear independence of the functions $t \mapsto \exp(\imath m \omega t)$ yields a coupled nonlinear system for the functions $\{p_0^N, v_0^N, \cdots, p_N^N, v_N^N\}$. Additionally, each of the individual functions p_m^N must satisfy the boundary conditions in (3.4). The 0-th equation is given by $\Delta p_0^N = 0$, which together with the 0-th boundary

condition (and the fact that $\gamma > 0$) implies that p_0^N vanishes. By dividing the resulting PDEs by $m^2\omega^2$, we arrive at the claimed coupled system.

We observe that without the sums over k on the right-hand side of the system in Proposition 3.1, the system would be triangular and could be solved by substitution. One way of obtaining a triangular form is by linearizing the right-hand side as we show next.

3.2. A linearized multiharmonic cut-off algorithm. Next, we propose a linearized multilevel method. That is, for $N \ge 1$, we consider the sequence of the following linearized equations where the quadratic terms are approximated by taking into account N-1 harmonics:

$$(3.5) \begin{cases} p_{tt}^{N} - c^{2}\Delta p^{N} - b\Delta p_{t}^{N} \\ = \eta \operatorname{Proj}_{X_{N}} \left[((p^{N-1})^{2})_{tt} \right] + c^{2}\rho_{0}n_{0}v^{N} + \operatorname{Proj}_{X_{N}}h & \text{in } \Omega \times (0, T), \\ \beta p_{t}^{N} + \gamma p^{N} + \nabla p^{N} \cdot \boldsymbol{n} = 0 & \text{on } \partial\Omega \times (0, T), \\ v_{tt}^{N} + \delta\omega_{0}v_{t}^{N} + \omega_{0}^{2}v^{N} \\ = -\mu p^{N-1} + \operatorname{Proj}_{X_{N}} \left[\zeta(v^{N-1})^{2} + \xi \left(2v^{N}v_{tt}^{N-1} + (v_{t}^{N-1})^{2} \right) \right] & \text{in } \Omega \times (0, T), \end{cases}$$

where for $u^N \in X_N$, we formally define $u_m^N = 0$ for all m > N. To start the algorithm, we set $p^0 = 0$ and $v^0 = 0$. We next show that this problem can be seen as a triangular system of Helmholtz problems and algebraic equations that can be solved by successive substitution.

Proposition 3.2. Let the assumptions of Theorem 2.1 hold with the acoustic source term assumed to have the form $h = g_{tt}$, where g is given in (3.1). Then, an equivalent formulation of the problem in (3.5) with $p^0 = v^0 = 0$ is given by the following coupled system:

$$\begin{split} m &= 0 : \begin{cases} (i) & p_0^N = 0, \\ (ii) & \omega_0^2 v_0^N = \frac{\zeta}{2} \left(v_0^{N-1} \right)^2 + \sum_{j=0}^{N-1} \left(\frac{\zeta}{2} - \frac{\xi \omega^2}{2} j^2 \right) \left| v_j^{N-1} \right|^2, \\ \\ m &= 1 : \begin{cases} (i) & -p_1^N - \frac{c^2 + \imath b \omega}{\omega^2} \Delta p_1^N + c^2 \rho_0 n_0 v_1^N = -h_1^N - \eta \sum_{k=3:2}^{2N-3} \overline{p_{\frac{N-1}{2}}^{N-1}} p_{\frac{N+1}{2}}^{N-1}, \\ \\ (ii) & \left(-\omega^2 + \imath \delta \omega_0 \omega + \omega_0^2 \right) v_1^N + \mu p_1^{N-1} \\ & = \left(\zeta - \xi \omega^2 \right) v_0^{N-1} v_1^{N-1} + \sum_{k=1:2}^{2N-3} \left(\zeta - \xi \omega^2 \frac{k^2 + 3}{4} \right) \overline{v_{\frac{N-1}{2}}^{N-1}} v_{\frac{k+1}{2}}^{N-1}, \end{split}$$

$$m = \{2, \dots, N\} : \begin{cases} (i) & -p_m^N - \frac{\left(c^2 + imb\omega\right)}{\omega^2 m^2} \Delta p_m^N + c^2 \rho_0 n_0 v_m^N \\ & = -h_m^N - \frac{\eta}{2} \left(\sum_{l=1}^{m-1} p_l^{N-1} p_{m-l}^{N-1} - 2 \sum_{k=m+2:2}^{2(N-1)-m} \overline{p_{\frac{k-m}{2}}^{N-1}} p_{\frac{k+m}{2}}^{N-1}\right), \\ (ii) & \left(-\omega^2 + i\delta\omega_0\omega + \omega_0^2\right) v_m^N + \mu p_m^{N-1} \\ & = \sum_{l=0}^m \left(\frac{\zeta}{2} - \frac{\xi\omega^2}{2} (m-l)(2m-l)\right) v_l^{N-1} v_{m-l}^{N-1} \\ & + \sum_{k=m:2}^{2(N-1)-m} \left(\zeta + \frac{\xi\omega^2(k^2 + 3m^2)}{4}\right) \overline{v_{\frac{k-m}{2}}^{N-1}} v_{\frac{k+m}{2}}^{N-1} \end{cases}$$

for $N \geq 1$. Additionally, each of the individual functions p_m^N , where $m \in \{1, ..., N\}$, should satisfy boundary conditions (3.4).

Proof. The statement follows analogously to before by applying the Ansatz given in (3.2) and making use of the expressions provided in [20, Lemma 3.1] for projections onto X_N of products of two functions in X_N .

4. Convergence of the linearized multiharmonic algorithm for real fields

We next wish to establish convergence of the iterative scheme in (3.5) as $N \to \infty$ in a suitable norm. To make writing more compact, we adopt the operator notation

$$<\mathcal{L}_1 p^N, \phi^N > := \int_0^T \int_{\Omega} \left(p_{tt}^N \phi^N + c^2 \nabla p^N \cdot \nabla \phi^N + b \nabla p_t^N \cdot \nabla \phi^N \right) \, \mathrm{d}x \mathrm{d}s$$

$$+ \int_0^T \int_{\partial \Omega} \left(c^2 (\beta p_t^N + \gamma p^N) + b (\beta p_{tt}^N + \gamma p_t^N) \right) \phi^N \, \mathrm{d}\Gamma \mathrm{d}s$$

and

$$<\mathcal{L}_2 v^N, \phi^N> := \int_0^T \int_{\Omega} \left(v_{tt}^N + \delta \omega_0 v_t^N + \omega_0^2 v^N\right) \phi^N \, \mathrm{d}x \mathrm{d}s.$$

Then the algorithm can be stated as follows. Given the previous iterate $(p^{N-1}, v^{N-1}) \in X_N \times X_N$, we compute (p^N, v^N) for $N \ge 1$ as the solution of

(4.1a)
$$\langle \mathcal{L}_1 p^N, \phi^N \rangle = \int_0^T \int_{\Omega} \left(\eta((p^{N-1})^2)_{tt} + c^2 \rho_0 n_0 v_{tt}^N + h \right) \phi^N \, \mathrm{d}x \mathrm{d}s,$$

and

(4.1b)
$$\langle \mathcal{L}_2 v^N, \phi^N \rangle = \int_0^T \int_{\Omega} \left\{ -\mu p^{N-1} + \zeta (v^{N-1})^2 + \xi \left(2v^{N-1} v_{tt}^{N-1} + (v_t^{N-1})^2 \right) \right\} \phi^N \, \mathrm{d}x \mathrm{d}s,$$

for all $\phi^N \in X_N$. Note that (4.1b) can be solved first for v^N , which can then be used as input for solving (4.1a) for p^N . We can mimic the proof of Theorem 2.1 to show by induction that for each $N \ge 1$, problem (4.1) has a unique solution $(p^N, v^N) \in X_N \times X_N$ such that

$$||p^N||_{\mathcal{X}_p} \le r_p, \quad ||v^N||_{\mathcal{X}_v} \le r_v.$$

For fixed $N \ge 1$, unique solvability of the pressure equation can be established as in [21, Sec. 3] using Galerkin approximations in the space

$$X_{NJ} = \left\{ \Re \left\{ \sum_{m=1}^{N} \exp(im\omega t) u_m(x) \right\} : u_m \in \operatorname{span} \left\{ \phi_{m1}, \dots, \phi_{mJ} \right\} \right\}$$

with basis functions $\{\phi_{mj}\}_{j\geq 1}$ given by the eigenfunctions of the Laplacian with frequency-dependent impedance boundary conditions

$$\begin{cases} -\Delta \phi_{mj} = \lambda_{mj} \phi_{mj} & \text{in } \Omega, \\ \nabla \phi_{mj} \cdot \boldsymbol{n} + i m \omega \beta \phi_{mj} + \gamma \phi_{mj} = 0 & \text{on } \partial \Omega, \end{cases}$$

and using suitable Galerkin testing. We omit those details here and focus on establishing convergence. The convergence will be shown in the norms of the spaces Y_p^0 and Y_v^0 , where

$$\begin{split} Y_p^{\ell} &= H^{\ell+1}(0,T;H^1(\Omega)) \cap H^{\ell+2}(0,T;L^2(\Omega)) \cap H^{\ell+2}(0,T;L^2(\partial\Omega)), \\ Y_v^{\ell} &= H^{\ell+2}(0,T;L^2(\Omega)) \end{split}$$

for $\ell \geq 0$. Let us also introduce the short-hand norm notation

$$|||(p,v)||_{Y_p^{\ell}\times Y_v^{\ell}} := ||p||_{Y_p^{\ell}} + ||v||_{Y_v^{\ell}}$$

for $(p, v) \in Y_p^{\ell} \times Y_v^{\ell}$.

In the convergence proof, we will involve the truncated Fourier series of a continuous-in-time function u given by

$$\tilde{u}^{N}(x,t) = \sum_{m=0}^{N} \left[u_{m}^{c}(x) \cos(m\omega t) + u_{m}^{s}(x) \sin(m\omega t) \right] \in X_{N}, \quad N \ge 0,$$

with the coefficients

$$u_m^c(x) = \frac{2}{T} \int_0^T u(x,t) \cos(m\omega t) dt, \quad u_m^s(x) = \frac{2}{T} \int_0^T u(x,t) \sin(m\omega t) dt.$$

By integrating the time-periodic Westervelt equation and acoustic boundary conditions in (2.1) over (0,T), we can conclude that $\int_0^T p(x,t) dt = 0$ in Ω . Thus $\tilde{p}^0 = 0$, which is reflected by having $p_0^N = 0$ in the multiharmonic algorithms.

It can be shown analogously to [3, Lemma 12] that the following error bound holds for $\ell \geq 1$:

which we can exploit to characterize the error of the scheme in the next statement. We include the proof of (4.2) in Appendix B for completeness.

Theorem 4.1. Let the assumptions of Theorem 2.1 hold with the acoustic source term $h = g_{tt}$, where g is given in (3.1). Assume additionally that

$$(p,v) \in \left(\mathcal{X}_p \cap Y_p^{\ell} \cap H^{\ell+2}(0,T;H^1(\Omega))\right) \times \left(\mathcal{X}_v \cap Y_v^{\ell}\right), \quad \ell \ge 1.$$

Let $p^0 = v^0 = 0$ and assume that (p^N, v^N) are computed using (4.1) for $N \ge 1$. Then, provided r_p , r_v , and $\|\mu\|_{L^{\infty}(\Omega)}$ are sufficiently small, there exists $q = q(r_p, r_v, \mu) < 1$, such

that

where C > 0 does not depend on N.

Proof. The proof follows by splitting the error as follows:

$$p - p^{N} = (p - \tilde{p}^{N}) - (p^{N} - \tilde{p}^{N}) =: \operatorname{err}(\tilde{p}^{N}) - e^{p,N},$$

$$v - v^{N} = (v - \tilde{v}^{N}) - (v^{N} - \tilde{v}^{N}) =: \operatorname{err}(\tilde{v}^{N}) - e^{v,N},$$

and then representing $(e^{p,N}, e^{v,N})$ as the solution of a suitable semi-discrete wave-volume system. The discrete error $(e^{p,N}, e^{v,N})$ can be seen as the solution of

(4.4a)
$$<\mathcal{L}_1 e^{p,N}, \phi^N> = -\int_0^T \int_{\Omega} \left(\eta(p^2 - (p^{N-1})^2)_{tt} + c^2 \rho_0 n_0 (v_{tt} - v_{tt}^N) \right) \phi^N \, dx ds + <\mathcal{L}_1 \operatorname{err}(\tilde{p}^N), \phi^N >$$

and

$$\langle \mathcal{L}_{2}e^{v,N}, \phi^{N} \rangle$$

$$= -\int_{0}^{T} \int_{\Omega} \left(-\mu(p - p^{N-1}) + \zeta(v^{2} - (v^{N-1})^{2}) + \xi(2(vv_{tt} - v^{N-1}v_{tt}^{N-1}) + (v_{t}^{2} - (v_{t}^{N-1})^{2})) \right) \phi^{N} \, \mathrm{d}x \mathrm{d}s$$

$$+ \langle \mathcal{L}_{2}\mathrm{err}(\tilde{v}^{N}), \phi^{N} \rangle$$

for all $\phi^N \in X_N$. Note that in the testing procedure for this problem we can exploit the fact that $\int_0^T \frac{\mathrm{d}}{\mathrm{d}t}(\cdot) \, \mathrm{d}t = 0$ for time-periodic functions. By testing (4.4a) with $e^{p,N}$, $e^{p,N}_t$, and $e^{p,N}_{tt}$, employing Young's and Hölder's inequalities, and combining the resulting estimates, we can derive the following bound:

(4.5)
$$\|e^{p,N}\|_{Y_p^0}^2 \lesssim \|-\eta(p^2 - (p^{N-1})^2)_{tt} - c^2 \rho_0 n_0 (v_{tt} - v_{tt}^N)\|_{L^2(L^2(\Omega))}^2 + \|\operatorname{err}(\tilde{p}^N)\|_{Y_p^0 \cap H^2(H^1(\Omega))}^2,$$

where we have also exploited the equivalence of the norms $||w||_{H^1(\Omega)}$ and $||\nabla w||_{L^2(\Omega)} + ||w||_{L^2(\partial\Omega)}$ (see [29, Theorem 1.9]). The derivation of (4.5) is provided in Appendix C. Then by using the rewriting

$$((p^{N-1})^2)_{tt} - (p^2)_{tt} = 2(p_t^{N-1} - p_t)(p_t^{N-1} + p_t) + 2(p^{N-1} - p_t)p_{tt}^{N-1} + 2p(p_{tt}^{N-1} - p_{tt}),$$

and the fact that $\|p\|_{\mathcal{X}_p}$, $\|p^N\| \le r_p$ for all $N \ge 1$, we obtain

$$||e^{p,N}||_{Y_p^0} \lesssim ||\eta||_{L^{\infty}(\Omega)} r_p ||p^{N-1} - p||_{Y_p^0} + ||n_0||_{L^{\infty}(\Omega)} ||v_{tt}^N - v_{tt}||_{L^2(L^2(\Omega))} + ||\operatorname{err}(\tilde{p}^N)||_{Y_p^0 \cap H^2(H^1(\Omega))}.$$

From here via $p - p^N = \text{err}(\tilde{p}^N) - e^{p,N}$ and the triangle inequality, we arrive at

$$(4.6) ||p-p^N||_{Y_p^0} \lesssim ||\eta||_{L^{\infty}(\Omega)} r_p ||p^{N-1}-p||_{Y_p^0} + ||n_0||_{L^{\infty}(\Omega)} ||v_{tt}^N-v_{tt}||_{L^2(L^2(\Omega))} + ||\operatorname{err}(\tilde{p}^N)||_{Y_p^0 \cap H^2(H^1(\Omega))}.$$

Similarly, testing (4.4b) with $e^{v,N}$, $e_t^{v,N}$, and $e_{tt}^{v,N}$ yields, after standard manipulations,

$$\begin{aligned} \|e^{v,N}\|_{Y_v^0}^2 \lesssim \|\mu(p-p^{N-1})\|_{L^2(L^2(\Omega))}^2 + \|-\zeta(v^2-(v^{N-1})^2)\|_{L^2(L^2(\Omega))}^2 \\ & \|-\xi(2(vv_{tt}-v^{N-1}v_{tt}^{N-1})+(v_t^2-(v_t^{N-1})^2))\|_{L^2(L^2(\Omega))}^2 + \|\operatorname{err}(\tilde{v}^N)\|_{Y_v^0}^2. \end{aligned}$$

By using the fact that $||v||_{\mathcal{X}_v}$, $||v^N||_{\mathcal{X}_v} \leq r_v$ for all $N \geq 1$, and the triangle inequality, from (4.4b) we then have

By using this estimate in (4.6), we conclude that

$$(4.8) ||p - p^{N}||_{Y_{p}^{0}} \lesssim (||\eta||_{L^{\infty}(\Omega)}r_{p} + ||n_{0}||_{L^{\infty}(\Omega)}||\mu||_{L^{\infty}(\Omega)})||p^{N-1} - p||_{Y_{p}^{0}} + ||n_{0}||_{L^{\infty}(\Omega)}(||\zeta||_{L^{\infty}(\Omega)} + ||\xi||_{L^{\infty}(\Omega)})r_{v}||v^{N-1} - v||_{Y_{v}^{0}} + ||\operatorname{err}(\tilde{p}^{N})||_{Y_{p}^{0} \cap H^{2}(H^{1}(\Omega))} + ||n_{0}||_{L^{\infty}(\Omega)}||\operatorname{err}(\tilde{v}^{N})||_{Y_{v}^{0}}.$$

Adding (4.7) and (4.8) then yields

$$(4.9) \qquad \|p-p^{N}\|_{Y_{p}^{0}} + \|v-v^{N}\|_{Y_{v}^{0}}$$

$$\lesssim (\|\eta\|_{L^{\infty}(\Omega)}r_{p} + (1+\|n_{0}\|_{L^{\infty}(\Omega)})\|\mu\|_{L^{\infty}(\Omega)})\|p^{N-1} - p\|_{Y_{p}^{0}}$$

$$+ (1+\|n_{0}\|_{L^{\infty}(\Omega)})(\|\zeta\|_{L^{\infty}(\Omega)} + \|\xi\|_{L^{\infty}(\Omega)})r_{v}\|v^{N-1} - v\|_{Y_{v}^{0}}$$

$$+ \|\operatorname{err}(\tilde{p}^{N})\|_{Y_{p}^{0} \cap H^{2}(H^{1}(\Omega))} + (1+\|n_{0}\|_{L^{\infty}(\Omega)})\|\operatorname{err}(\tilde{v}^{N})\|_{Y_{v}^{0}}.$$

Let C_0 be the hidden constant above and let

$$q(r_p, r_v, \mu) := C_0 \{ \|\eta\|_{L^{\infty}(\Omega)} r_p + (1 + \|n_0\|_{L^{\infty}(\Omega)}) \|\mu\|_{L^{\infty}(\Omega)} + (1 + \|n_0\|_{L^{\infty}(\Omega)}) (\|\xi\|_{L^{\infty}(\Omega)} + \|\xi\|_{L^{\infty}(\Omega)}) r_v \}.$$

By possibly further reducing r_p , r_v , and $\|\mu\|_{L^{\infty}(\Omega)}$, we have $q(r_p, r_v, \mu) < 1$. Thus from (4.9) we obtain

$$\begin{aligned} \|(p-p^N, v-v^N)\|_{Y_p^0 \times Y_v^0} &\leq q(r_p, r_v, \mu) \|(p-p^{N-1}, v-v^{N-1})\|_{Y_p^0 \times Y_v^0} \\ &\qquad \qquad + (1+\|n_0\|_{L^{\infty}(\Omega)})C_0 \|(\operatorname{err}(\tilde{p}^N), \operatorname{err}(\tilde{v}^N))\|_{\left(Y_p^0 \cap H^2(H^1(\Omega))\right) \times Y_v^0}. \end{aligned}$$

The statement then follows by employing (4.2).

Convergence of the scheme then follows in a straightforward manner from (4.5).

Corollary 1 (Convergence of the linearized scheme). Let the assumptions of Theorem 4.1 hold. Then the solution $(p^N, v^N) \in X_N \times X_N$ of the iteration scheme (4.1) converges with respect to the norm $\|(\cdot, \cdot)\|_{Y_p \times Y_v}$ to the solution $(p, v) \in \mathbb{B}_{r_p, r_v}$ of (2.1) as $N \to \infty$.

Proof. From (4.5), by iteration we obtain

$$\begin{aligned} \| (p - p^N, v - v^N) \|_{Y_p^0 \times Y_v^0} &\leq q(r_p, r_v, \mu)^N \| (p - p^0, v - v^0) \|_{Y_p^0 \times Y_v^0} \\ &+ C \sum_{i=1}^N q(r_p, r_v, \mu)^{N-1} \| (p - \tilde{p}^i, v - \tilde{v}^i) \|_{Y_p^0 \times Y_v^0} \end{aligned}$$

for some C > 0, independent of N. The statement then follows analogously to [31, Theorem 3.1], where the multiharmonic discretization of the de-coupled Westervelt equation is studied. We thus omit the details here.

Setting v_0^N to zero for all $N \geq 0$. Note that, unlike with the Westervelt equation, from the equation for v, we cannot in general conclude by integrating from 0 to T that $\int_0^T v(t) \, \mathrm{d}t = 0$. Nevertheless, in numerical methods for solving multiharmonic problems it is often assumed that the zeroth harmonic does not contribute significantly to the dynamics; this assumption is also made in the formal two-harmonic generation study for the linearized wave-ODE model with $b = \eta = 0$ in [16, Ch. 5.3.2].

With the assumption $p_0^N = v_0^N = 0$ for all $N \ge 0$, the system derived in Proposition 3.2 further simplifies to

$$(4.10) \qquad m=1: \begin{cases} \text{(i)} & -p_1^N - \frac{c^2 + \imath b \omega}{\omega^2} \Delta p_1^N + c^2 \rho_0 n_0 v_1^N = -h_1^N - \sum_{k=3:2}^{2N-3} \eta \overline{p_{\frac{N-1}{2}}^{N-1}} p_{\frac{k+1}{2}}^{N-1} \\ \text{(ii)} & v_1^N = \alpha_1 \left(-\mu p_1^{N-1} + \sum_{k=3:2}^{2N-3} \left(\zeta - \xi \omega^2 \frac{k^2 + 3}{4} \right) \overline{v_{\frac{k-1}{2}}^{N-1}} v_{\frac{k+1}{2}}^{N-1} \right) \\ & = \left(\text{(i)} & -p_m^N - \frac{\left(c^2 + \imath m b \omega \right)}{\omega^2 m^2} \Delta p_m^N + c^2 \rho_0 n_0 v_m^N \\ & = -h_m^N - \frac{\eta}{2} \left(\sum_{l=1}^{m-1} p_l^{N-1} p_{m-l}^{N-1} - 2 \sum_{k=m+2:2}^{2(N-1)-m} \overline{p_{\frac{k-m}{2}}^{N-1}} p_{\frac{k+m}{2}}^{N-1} \right) \\ & = -h_m^N - \frac{\eta}{2} \left(\sum_{l=1}^{m-1} p_l^{N-1} p_{m-l}^{N-1} - 2 \sum_{k=m+2:2}^{2(N-1)-m} \overline{p_{\frac{k-m}{2}}^{N-1}} p_{\frac{k+m}{2}}^{N-1} \right) \\ & + \sum_{k=m+2:2}^{2(N-1)-m} \left(\zeta + \frac{\xi \omega^2 (k^2 + 3m^2)}{4} \right) \overline{v_{\frac{k-m}{2}}^{N-1}} v_{\frac{k+m}{2}}^{N-1} \right) \end{cases}$$

where

$$\alpha_m = \frac{1}{-\omega^2 + i\delta\omega_0\omega + \omega_0^2}.$$

Note that v_m^N can be eliminated explicitly by substituting the second equation into the first, leading to a system of inhomogeneous Helmholtz equations.

5. Time discretization via a multiharmonic Ansatz for complex fields

In this section, we formally investigate multiharmonic algorithms based on neglecting the fact that the excitation and solution fields should be real-valued. We look for approximate solutions in

$$\tilde{X}_N := \left\{ \sum_{m=0}^N \exp(\imath m \omega t) u_m^N(x) \ : \ u_m^N \in H^2(\Omega; \mathbb{C}) \right\}.$$

This approach, adopted also in the investigation of the (de-coupled) Westervelt equation in [20], will allow us to arrive at a simple triangular approximation scheme in the frequency

domain. To this end, we simply set

(5.1)
$$g^{M}(x,t) = \sum_{m=0}^{M} \exp(i\omega mt) h_{m}^{M}(x), \quad \omega = \frac{2\pi}{T},$$

and make the following Ansatz:

(5.2)
$$p^{N}(x,t) = \sum_{m=0}^{N} \exp(im\omega t) p_{m}^{N}(x), \quad v^{N}(x,t) = \sum_{m=0}^{N} \exp(im\omega t) v_{m}^{N}(x),$$

where the coefficients p_m^N , $v_m^N \in H^2(\Omega; \mathbb{C})$ are determined by solving (3.3) with $\operatorname{Proj}_{X_N}(\cdot)$ replaced by $\operatorname{Proj}_{\tilde{X}_N}(\cdot)$.

5.1. A multiharmonic cut-off algorithm. We next set up a simplified algorithm (compared to the one in Proposition 3.1) in the sense that the right-hand side in the resulting system will contain only one summation term, such that there is reduced coupling across harmonics, making it computational more efficient.

In this complex setting, for v_0^N , we obtain the quadratic equation

$$\omega_0^2 v_0^N - \zeta(v_0^N)^2 = 0$$

and choose the zero solution, such that we have $v_0^N=0$ as before in (4.10). This choice is consistent with the formulation used throughout the numerical simulations and avoids introducing spurious constant components.

Proposition 5.1. Let the assumptions of Theorem 2.1 hold with the acoustic source term $h = g_{tt}$, where g is given in (5.1). Under the Ansatz in (5.2) with $p_0^N = v_0^N = 0$, the problem in (3.3) with $\operatorname{Proj}_{X_N}(\cdot)$ replaced by $\operatorname{Proj}_{\tilde{X}_N}(\cdot)$ can be rewritten as follows:

(5.3)
$$m = 1: \begin{cases} (i) & -p_1^N - \frac{c^2 + i\omega b}{\omega^2} \Delta p_1^N + c^2 \rho_0 n_0 v_1^N = -h_1^N \\ (ii) & \left(-\omega^2 + \delta \omega_0 i\omega + \omega_0^2\right) v_1^N + \mu p_1^N = 0 \end{cases}$$

$$m = \{2, \dots, N\} : \begin{cases} (i) & -p_m^N - \frac{(c^2 + \imath m \omega b)}{m^2 \omega^2} \Delta p_m^N + c^2 \rho_0 n_0 v_m^N = -h_m^N - \eta \sum_{l=1}^{m-1} p_l^N p_{m-l}^N \\ (ii) & \left(-m^2 \omega^2 + \delta \omega_0 \imath m \omega + \omega_0^2 \right) v_m^N + \mu p_m^N = \sum_{l=1}^{m-1} \left(\zeta - \xi \omega^2 (m-l) (2m-l) \right) v_l^N v_{m-l}^N. \end{cases}$$

Additionally, each of the individual functions p_m^N , where $m \in \{0, ..., N\}$, should satisfy boundary conditions (3.4).

Proof. Plugging the approximation given in (5.2) into (2.1) yields

$$\begin{split} \sum_{m=0}^{N} \left[-m^{2}\omega^{2}p_{m}^{N} - (c^{2} + \imath m\omega b)\Delta p_{m}^{N} + c^{2}\rho_{0}n_{0}m^{2}\omega^{2}v_{m}^{N} + m^{2}\omega^{2}h_{m}^{N} \right. \\ \left. + \sum_{l=0}^{m} \eta m^{2}\omega^{2}p_{l}^{N}p_{m-l}^{N} \right] \exp(\imath m\omega t) = 0. \end{split}$$

Concerning the nonlinear term on the right hand-side of the ODE, we obtain

$$\operatorname{Proj}_{\tilde{X}_{N}}(2v^{N}v_{tt}^{N} + (v_{t}^{N})^{2}) = -\sum_{m=0}^{N} \sum_{l=0}^{m} (2(m-l)^{2} + l(m-l)) \omega^{2} v_{l}^{N} v_{m-l}^{N} \exp(\imath m \omega t)$$

$$= -\sum_{m=0}^{N} \sum_{l=0}^{m} (m-l)(2m-l) \omega^{2} v_{l}^{N} v_{m-l}^{N} \exp(\imath m \omega t).$$

Therefore, the approximation for the ODE is given by

$$\sum_{m=0}^{N} \left[\left(-m^2 \omega^2 + \delta \omega_0 \imath m \omega + \omega_0^2 \right) v_m^N + \mu p_m^N + \sum_{l=0}^{m} \left(-\zeta + \xi \omega^2 (m-l) (2m-l) \right) v_l^N v_{m-l}^N \right] \exp(\imath m \omega t) = 0.$$

Using linear independence of the functions $t \mapsto \exp(im\omega t)$, we immediately arrive at the iterative coupled system.

5.2. A linearized multiharmonic cut-off algorithm. We next also want to look at the linearized set-up given in (3.5) (with $\operatorname{Proj}_{X_N}(\cdot)$ replaced by $\operatorname{Proj}_{\tilde{X}_N}(\cdot)$) in the setting of complex solution fields. In this setting, for $u^N \in \tilde{X}_N$, we formally define $u_m^N = 0$ for all m > N.

Proposition 5.2. Let the assumptions of Theorem 2.1 hold with the acoustic source term $h = g_{tt}$, where g is given in (5.1). Under the Ansatz in (5.2) with $p_0^N = v_0^N = 0$, the problem in (3.5), with $\operatorname{Proj}_{X_N}(\cdot)$ replaced by $\operatorname{Proj}_{\tilde{X}_N}(\cdot)$, can be rewritten as follows:

$$(5.4)$$

$$m = 1: \begin{cases} (i) & -p_1^N - \frac{c^2 + \imath \omega b}{\omega^2} \Delta p_1^N + c^2 \rho_0 n_0 v_1^N = -h_1^N, \\ (ii) & \left(-\omega^2 + \delta \omega_0 \imath \omega + \omega_0^2\right) v_1^N + \mu p_1^{N-1} = 0, \end{cases}$$

$$m = \{2, \dots, N\}: \begin{cases} (i) & -p_m^N - \frac{\left(c^2 + \imath m \omega b\right)}{m^2 \omega^2} \Delta p_m^N + c^2 \rho_0 n_0 v_m^N = -h_m^N - \frac{\beta_a}{\rho_0 c^2} \sum_{l=1}^{m-1} p_l^{N-1} p_{m-l}^{N-1}, \\ (ii) & \left(-m^2 \omega^2 + \delta \omega_0 \imath m \omega + \omega_0^2\right) v_m^N + \mu p_m^{N-1} \\ & = \sum_{l=1}^{m-1} \left(\zeta - \xi \omega^2 (m-l)(2m-l)\right) v_l^{N-1} v_{m-l}^{N-1}. \end{cases}$$

Additionally, each of the individual functions p_m^N for $m \in \{0, ..., N\}$ is supposed to satisfy boundary conditions (3.4).

Proof. Similarly to the previous case, substituting the approximation provided in (5.2) into (2.1) immediately yields the iterative coupled system.

We see that when working with complex fields from the beginning, we end up with a lower triangular system of inhomogeneous Helmholtz equations and algebraic equations that can be solved by substitution. Remark 1 (On the assumption of complex fields). Since approximations of the pressurevolume field in this section are complex-valued, convergence occurs within the complex counterpart of the space $X_N \times X_N$, which limits their practical applicability to realvalued functions. We cannot conclude that the real part of (p^N, v^N) converges to (p, v) as $N \to \infty$. Additionally, as discussed in [3], complex formulation leads to functions that are not complex differentiable, thus precluding the use of Newton methods. For this reason, real-valued formulations might be preferable despite the algebraic simplicity of the complex setting. Nevertheless, our numerical investigations in Section 6, where we compare the algorithms in this section with those of Section 3 do not show noticeable qualitative differences between the resulting solutions fields in the considered simulation setting.

5.3. A two-harmonic approximation scheme. In certain imaging applications, the fundamental frequency and the second harmonic are considered the most significant; see, e.g., [35]. We thus compare the multiharmonic iterative scheme with a simplified two-harmonic scheme to evaluate the extent of information loss.

harmonic scheme to evaluate the extent of information loss. For two harmonics, that is, for N=2 with $p_0^{(2)}=0$ and $v_0^{(2)}=0$, the approximations for the pressure p and the volume v are given by

$$p(x,t) \approx p^{(2)}(x,t) = p_1^{(2)}(x) \exp(\imath \omega t) + p_2^{(2)}(x) \exp(2\imath \omega t),$$

$$v(x,t) \approx v^{(2)}(x,t) = v_1^{(2)}(x) \exp(\imath \omega t) + v_2^{(2)}(x) \exp(2\imath \omega t).$$

The corresponding scheme for computing $p_{1,2}^{(2)}$ and $v_{1,2}^{(2)}$ can be found by setting N=2 in Proposition 5.1. This results in the system

$$m = 1: \begin{cases} (i) & p_1^{(2)} + \frac{c^2 + \imath \omega b}{\omega^2} \Delta p_1^{(2)} - c^2 \rho_0 n_0 v_1^{(2)} = h_1^{(2)}, \\ (ii) & \left(-\omega^2 + \delta \omega_0 \imath \omega + \omega_0^2 \right) v_1^{(2)} + \mu p_1^{(2)} = 0, \end{cases}$$

$$(5.5)$$

$$m = 2: \begin{cases} (i) & p_2^{(2)} + \frac{\left(c^2 + 2\imath \omega b\right)}{4\omega^2} \Delta p_2^{(2)} - c^2 \rho_0 n_0 v_2^{(2)} = h_2^{(2)} + \frac{\beta_a}{\rho_0 c^2} (p_1^{(2)})^2, \\ (ii) & \left(-4\omega^2 + 2\delta \omega_0 \imath \omega + \omega_0^2 \right) v_2^{(2)} + \mu p_2^{(2)} = \left(\zeta - 3\xi \omega^2 \right) (v_1^{(2)})^2. \end{cases}$$

Above, we have rewritten η as $\eta = \frac{\beta_a}{\rho_0 c^2}$ to make the influence of the nonlinearity parameter in the medium β_a on the system explicit. In this two-harmonic setting, we can express $v_1^{(2)}$ in terms of $p_1^{(2)}$ and $v_2^{(2)}$ in terms of $p_2^{(2)}$:

(5.6)
$$v_1^{(2)} = -\alpha_1 \mu \, p_1^{(2)},$$

$$v_2^{(2)} = \alpha_2 \left[-\mu p_2^{(2)} + (\zeta - 3\xi\omega^2) \tilde{\alpha}_1^2 \mu^2 \left(p_1^{(2)} \right)^2 \right],$$

where

$$\alpha_m = \frac{1}{-m^2\omega^2 + m\delta\omega_0\imath\omega + \omega_0^2}, \quad m \in \{1, 2\}.$$

We can then use these expressions to eliminate $v_1^{(2)}$ and $v_2^{(2)}$ for the first and third equations in (5.5). Multiplying the resulting equations by $m^2\omega^2/c^2$ yields the following system

for the two pressure coefficients:

(5.7)
$$m = 1: \qquad \frac{\omega^2}{\tilde{c}_1^2} p_1^{(2)} + \left(1 + \frac{\imath b\omega}{c^2}\right) \Delta p_1^{(2)} = \frac{\omega^2}{c^2} h_1^{(2)},$$
$$m = 2: \qquad \frac{4\omega^2}{\tilde{c}_2^2} p_2^{(2)} + \left(1 + \frac{2\imath b\omega}{c^2}\right) \Delta p_2^{(2)} = \frac{4\omega^2}{c^2} h_2^{(2)} + \frac{4\omega^2}{\rho_0 c^4} \left(\beta_a + \tilde{\beta}\right) \left(p_1^{(2)}\right)^2,$$

where

$$\frac{1}{\tilde{c}_m^2} = \frac{1}{c^2} + \rho_0 n_0 \alpha_m \mu, \qquad \tilde{\beta} = c^4 \rho_0^2 n_0 (\zeta - 3\xi \omega^2) \mu^2 \alpha_1^2 \alpha_2.$$

The influence of microbubbles. The above system clearly displays the influence of microbubbles on wave evolution, particularly through their impact on the effective wave speed and the nonlinearity parameter.

• From equation (5.7), the squared wave number for the m-th harmonic is given by

$$\tilde{k}_m^2 = \frac{m^2 \omega^2}{\tilde{c}_m^2 \left(1 + \frac{\imath b m \omega}{c^2}\right)}.$$

This wave number is clearly complex-valued, due to both the imaginary damping term $\frac{ibm\omega}{c^2}$ and the fact that \tilde{c}_m itself is complex. The imaginary part of \tilde{k}_m leads to attenuation of the wave, as illustrated in Figure 7. We recall that in the classical Helmholtz equation, the wave number for the m-th harmonic is given by $k_m = \frac{m\omega}{c}$.

• In the second equation in (5.7), we see the influence of microbubbles on the nonlinearity parameter as their presence leads to the additional $\tilde{\beta}$ term on the right-hand side, thus effectively enlarging the nonlinearity parameter β_a . By setting $\tilde{\beta} = 0$ and replacing \tilde{c}_m^2 with c^2 , the system reduces to the two-harmonic expansion of Westervelt's equation for a strongly damped medium without bubbles.

An undamped linear wave setting. In Section 6, we also compare numerically our model to a coupled system of the same ODE with the undamped linear wave equation:

$$\frac{1}{c^2}p_{tt} - \Delta p = \rho_0 n_0 v_{tt} + h.$$

This problem has been formally studied in [16, Ch. 5], and a two-harmonic expansion algorithm is given by

$$m = 1: \qquad \frac{\omega^2}{c^2} p_1^{(2)} + \Delta p_1^{(2)} = \omega^2 \rho_0 n_0 v_1^{(2)} + \frac{\omega^2}{c^2} h_1^{(2)},$$

$$m = 2: \qquad \frac{4\omega^2}{c^2} p_2^{(2)} + \Delta p_2^{(2)} = 4\omega^2 \rho_0 n_0 v_2^{(2)} + \frac{4\omega^2}{c^2} h_2^{(2)}.$$

Substituting (5.6) into the above system yields

(5.8)
$$m = 1: \qquad \frac{\omega^2}{\tilde{c}_1^2} p_1^{(2)} + \Delta p_1^{(2)} = \frac{\omega^2}{c^2} h_1^{(2)}, \\ m = 2: \qquad \frac{4\omega^2}{\tilde{c}_2^2} p_2^{(2)} + \Delta p_2^{(2)} = \frac{4\omega^2}{c^2} h_2^{(2)} + \frac{4\omega^2}{\rho_0 c^4} \tilde{\beta} \left(p_1^{(2)} \right)^2,$$

where we also equip the two-harmonic expansion with the boundary conditions (3.4).

6. Numerical results

In this section, we investigate numerically the algorithms set up in Sections 3 and 5. To discretize the resulting Helmholtz problems, we use a conforming finite element method. Algorithmic frameworks of the multiharmonic-FEM type used in this section are known as the Harmonic Balance Finite Element Method (HBFEM) in the context of electromagnetism; see, e.g., [3, 4, 26]. We note that while the discretization of the Helmholtz equation has been extensively studied in the literature, see, e.g., [2, 18, 28], many of the classical rigorous results do not apply to our setting directly due to the presence of complex-valued wave numbers.

6.1. Numerical framework. All simulations are performed using a conforming twodimensional finite element discretization with linear Lagrange elements, using FEniCSx v0.9.0 (see, e.g., [5]) with Gmsh [13] employed for meshing.¹ We use a circular domain of propagation $\Omega = B_{0.2}(0) \subset \mathbb{R}^2$ with a radius of 0.2 m and place a monopole source h = h(x) at $x_0 = (0,0)^T$ defined as

$$h(x) = \begin{cases} \frac{a}{4r_{\delta}} \left(1 + \cos\left(\pi \frac{\|x - x_0\|_{l^2}}{2r_{\delta}}\right) \right) & \|x - x_0\|_{l^2} \le 2r_{\delta}, \\ 0 & \text{otherwise.} \end{cases}$$

We present results for different r_{δ} , a, and frequencies ω . The physical parameters used in the simulations are chosen as typical in ultrasound contrast imaging (see, e.g., [16, 17]), and are listed in Table 1.

Table 1. Overview of the parameter values used in the simulations.

Using the values in Table 1, we compute

$$\omega_0 = \sqrt{\frac{3\kappa P_0}{\rho_0 R_0^2}} \approx 0.324 \,\mathrm{MHz}$$

and additionally $\delta = \frac{4\nu}{\omega_0 R_0^2}$, $v_0 = \frac{4\pi}{3} R_0^3$, $\mu = \frac{4\pi R_0}{\rho_0}$, $\zeta = \frac{(\kappa+1)\omega_0^2}{2v_0}$, and $\xi = \frac{1}{6v_0}$ are fixed. Furthermore, we set $\beta = \tilde{c}_m$ and $\gamma = 1$ in the boundary conditions for Helmholtz problems.

6.2. Numerical evaluation. A common rule of thumb for finite element discretizations of the classical Helmholtz equation is to use at least 10 elements per wavelength in each spatial direction. If the mesh is not refined accordingly, one encounters the so-called pollution effect, where numerical phase errors grow with increasing k; see, e.g., [2, 18, 28]. In Figure 2, we plot a quantity of interest given by the $L^{\infty}(0,T;L^{2}(\Omega))$ norm of the

¹The program code for the simulations in this section is available as an ancillary file from the arXiv page of this paper.

pressure field for different mesh sizes h_{FEM} and different number of harmonics using the algorithm in (5.3). We see that as the mesh size h_{FEM} decreases, the quantity of interest approaches a value that varies with the number of harmonics N.

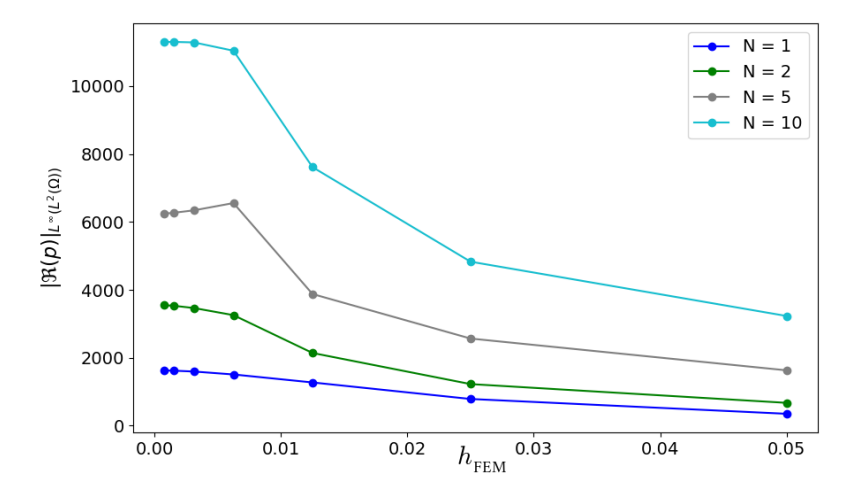


FIGURE 2. Dependence of the norm $\|\Re(p)\|_{L^{\infty}(L^2(\Omega))}$ on the mesh size h_{FEM} for different numbers of harmonics $N \in \{1, 2, 5, 10\}$; the pressure is computed using the scheme in (5.3) with $\omega = \omega_0$, $r_{\delta} = 0.004$, and A = 1500.

$h_{ m FEM}$	Nodes	Elements	Time
0.000390625	9,564,795	1,933,589	9984.8 s
0.00078125	239,024	478,047	$1244.3~\mathrm{s}$
0.0015625	60,136	$120,\!271$	$145.5~\mathrm{s}$
0.003125	$15,\!218$	$30,\!435$	$19.8 \mathrm{\ s}$
0.00625	3,896	7,791	$5.16 \mathrm{\ s}$
0.0125	1,010	2,019	$2.72 \mathrm{\ s}$
0.025	279	557	$2.24 \mathrm{\ s}$
0.05	85	169	$2.15 \mathrm{\ s}$

Table 2. Numerical data for different h_{FEM} values

Additional quantitative data are provided in Table 2, which lists the corresponding mesh sizes, number of nodes and elements, as well as the computational time required for each case. This highlights the significant increase in computational cost associated with finer meshes, especially for very small $h_{\rm FEM}$, where both the number of degrees of freedom and the runtime grow substantially. All simulations were carried out on a standard laptop (Intel Core i7, 16GB RAM, no dedicated GPU), underscoring the feasibility of the method even without access to high-performance computing resources.

In the following simulations, we use a mesh size of $h_{\text{FEM}} = 0.001$.

6.3. Multiharmonic approximation. Unless stated otherwise in the figure captions, we set $r_{\delta} = 0.004$, a = 1500, and $\omega = \omega_0$.

6.3.1. Comparison real- vs. complex-valued fields. Figure 3 shows the five-harmonic pressure obtained using the linearized multiharmonic cut-off algorithm for the complex field in (5.4) as well as for the real field in (4.10). In this numerical setting, we see that there are no noticeable differences between the two resulting pressure fields. However, the algorithm resulting from the complex setting is computationally more efficient, making it a more promising choice for simulations of real-world settings.

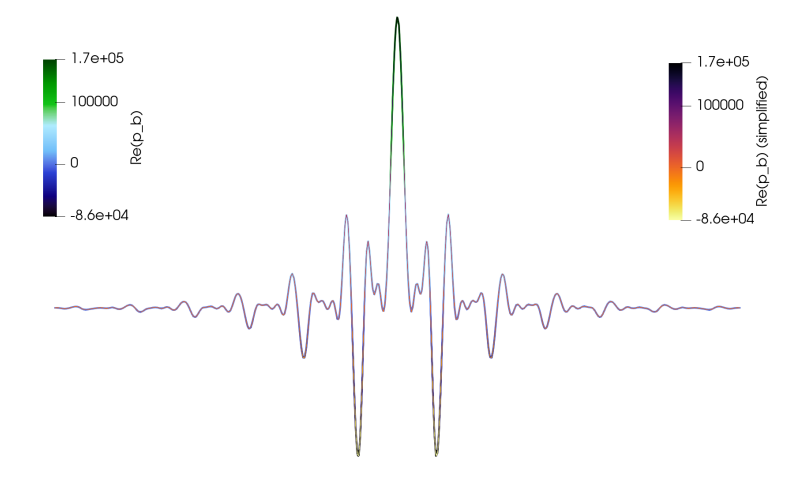
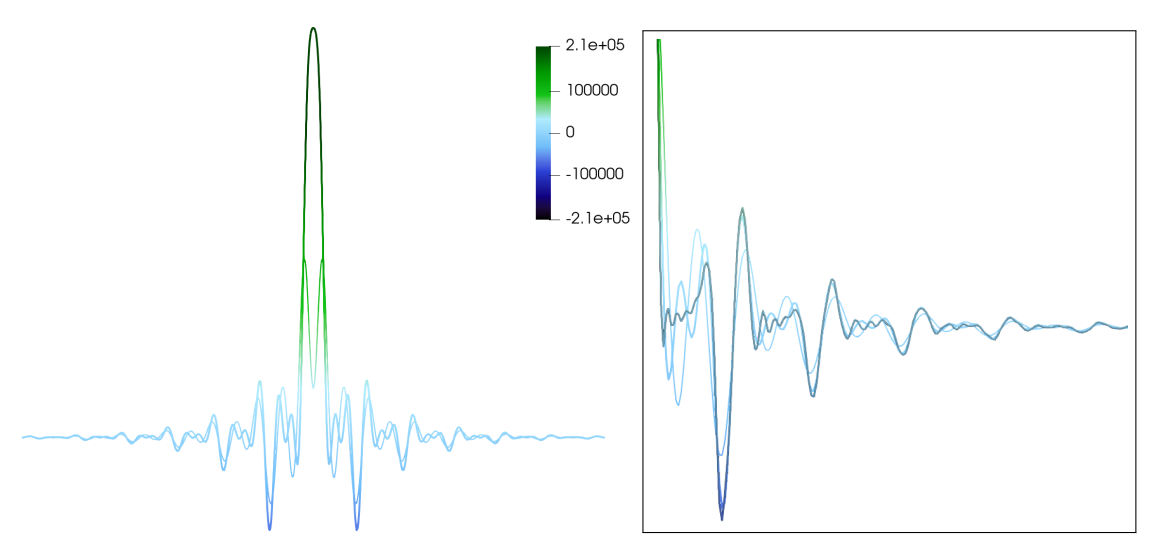


FIGURE 3. Five-harmonic expansion of $\Re(p(x, y_0, t_0))$ resulting from complex fields in (5.4) vs. real setting in (4.10).



(A) Two-harmonic expansion (thin line) vs. three-harmonic expansion (thick line).

(B) Close-up of the left plot with the tenharmonic expansion (gray) for comparison.

FIGURE 4. Real part of the pressure $\Re(p(x, y_0, t_0))$ obtained from (5.4) using complex fields for the two-, three- and ten-harmonic expansions.

6.3.2. The influence of the number of harmonics. Next, we compare the two-harmonic approximation to the multiharmonic setting. As shown in Figure 4, using only two harmonics results in a significant loss of information compared to the three-harmonic case. However, the difference between considering three and ten harmonics is relatively small in this setting. Since solving the system for ten harmonics is considerably more time-consuming, we found that using three to five harmonics provides a good balance between accuracy and computational efficiency for the considered parameter values.

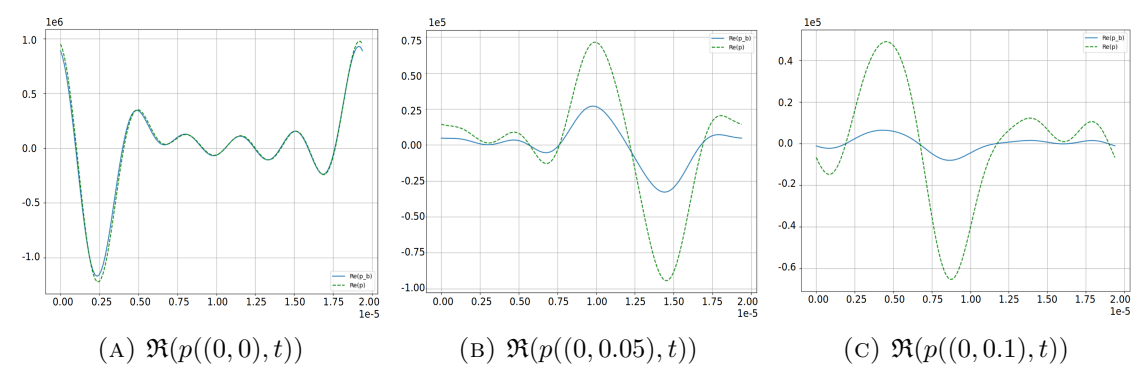


FIGURE 5. Real part of the pressure from the five-harmonic expansion computed using (5.4) without bubbles ($n_0 = 0$, dashed green line) and with bubbles (blue line) over time at three spatial points.

We further analyze the multiharmonic expansion by examining the temporal evolution of the five-harmonic expansion at different spatial points. As illustrated in Figure 5, the presence of microbubbles near the source has little effect on the pressure waves. However, as the distance from the source increases, the signal strength decreases, and the microbubbles not only attenuate the waveform but also enhance its nonlinear characteristics. To better visualize these effects, we scale the pressure waveform obtained from the five-harmonic expansion with bubbles to the maximum of the waveform without microbubbles, as shown in Figure 6.

6.4. **Two-harmonic approximation.** Finally, we focus on a two-harmonic setting to illustrate the influence of different parameters in the system. Unless stated otherwise in the figure captions, we set $r_{\delta} = 0.0005$, a = 5000, and $\omega = \omega_0$.

Figure 7 compares the real part of the pressure distribution within the domain at a specific time point with and without the presence of bubbles in the medium; that is, the real part of the pressure obtained using the algorithm in (5.7) and the same algorithm with $n_0 = \tilde{\beta} = 0$. The presence of bubbles leads to an overall damping effect, resulting in a reduced pressure amplitude across the domain. This observation aligns with the behavior predicted by the systems of equations in (5.8) and (5.7), as the modified speed of sound introduces attenuation. Although the source amplitude is fixed in this case, we note that the differences become more pronounced for larger source amplitudes, leading to higher overall pressure levels.

6.4.1. The influence of microbubble density. Figure 8 demonstrates the influence of the bubble number density n_0 on acoustic attenuation. A higher density, meaning more bubbles in the medium, leads to stronger attenuation compared to a lower density. A

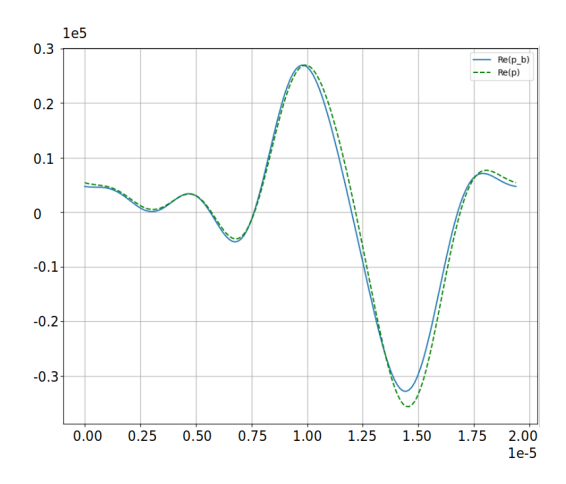
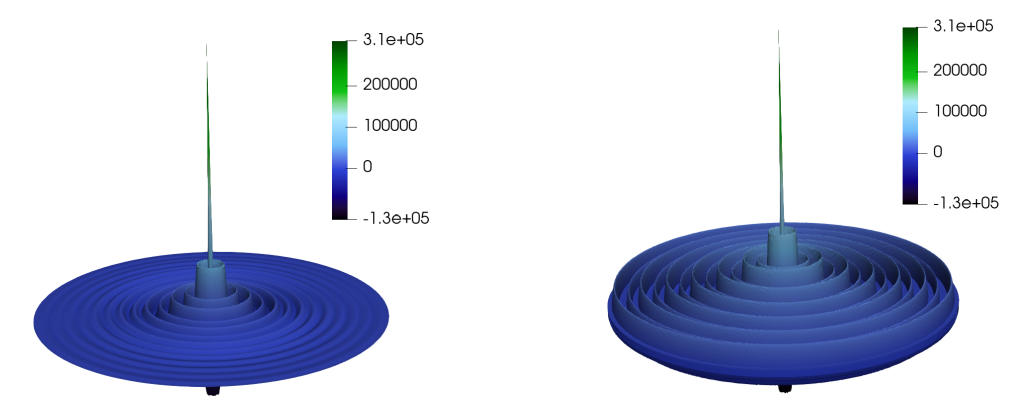


FIGURE 6. Real part of the pressure $\Re(p(0,0.05,t))$ from the five-harmonic expansion computed using (5.4) without bubbles ($n_0 = 0$, dashed green line) and with bubbles (blue line, scaled to the maximum of the green curve) over time.



- (A) Pressure with bubbles in the medium.
- (B) Pressure without bubbles in the medium.

FIGURE 7. Real part of the pressure $\Re(p(x, y, t_0))$ obtained using the two-harmonic scheme in (5.7).

noticeable effect of the bubbles only occurs above a certain relatively high density, in view of the fact that the results $n_0 = 5 \cdot 10^{10}$ and $n_0 = 0$ are very similar.

The behavior observed in space can also be seen over time, see Figure 9. Close to the source, the pressure in the bubbly medium remains nearly the same as in the bubble-free case. However, with increasing distance, the presence of bubbles causes progressively stronger damping, leading to greater attenuation further away from the source.

6.4.2. The influence of acoustic nonlinearities. Next, we compare the linear and nonlinear models in the presence of bubbles by analyzing the behavior of both pressure and radius fields at different spatial points over time; see Figure 10. We use the term linear model to refer specifically to the system in (5.8) derived from the linear wave equation and the term nonlinear model to refer to the system resulting from Westervelt's equation. The

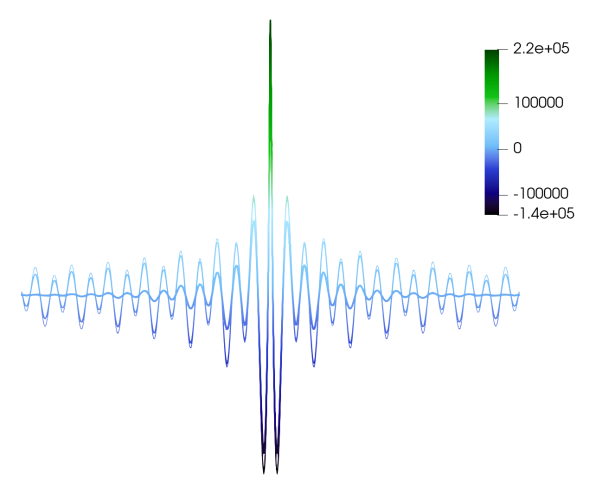


FIGURE 8. Real part of the pressure $\Re(p(x, y_0, t_0))$ obtained using the two-harmonic scheme given in (5.7) with varying bubble densities: high $(n_0 = 1 \cdot 10^{12}, \text{ thick})$, moderate $(n_0 = 5 \cdot 10^{10}, \text{ medium})$, and none (thin).

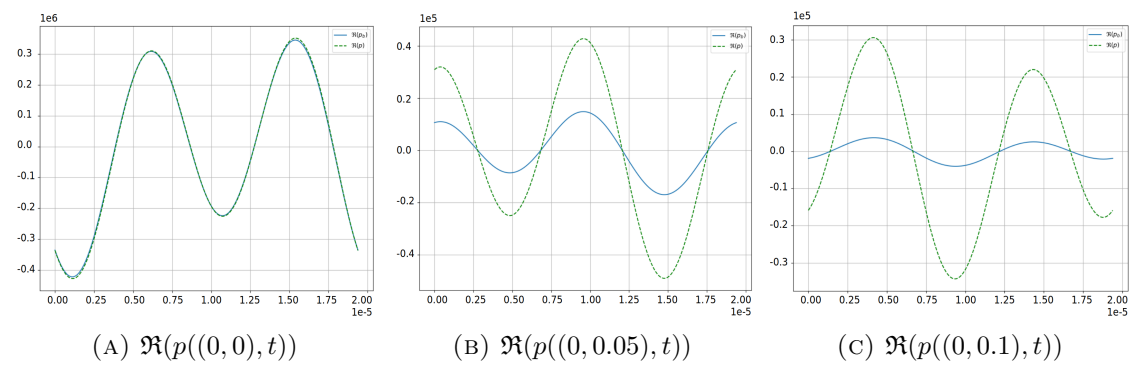


FIGURE 9. Real part of the pressure computed using the two-harmonic scheme (5.7) with microbubbles (blue line) and without microbubbles ($n_0 = 0$, dashed green) over time at three spatial points.

radius R has been calculated using $R = \sqrt[3]{\frac{3V}{4\pi}}$ with $V = v_0 + v$.

As expected, the effects of Westervelt's equation become more noticeable at greater distances from the source. The two models align closely near the source, but they start to differ as the wave propagates. As pressure decreases, the bubble radius also approaches its equilibrium state.

6.4.3. Changes in the driving frequency. Finally, we also want to present the case where the driving frequency does not correspond to the resonance frequency. The results in Figure 11 indicate that changing the driving frequency affects both the amplitude and the oscillatory structure of the pressure. For a lower driving frequency the waveform appears smoother with fewer oscillations. While one might expect resonance to yield the highest pressure amplitude, this is not the case here. Instead, the dominant factor influencing the amplitude is the source term, which includes a prefactor of ω^2 , leading to a stronger dependence on frequency.

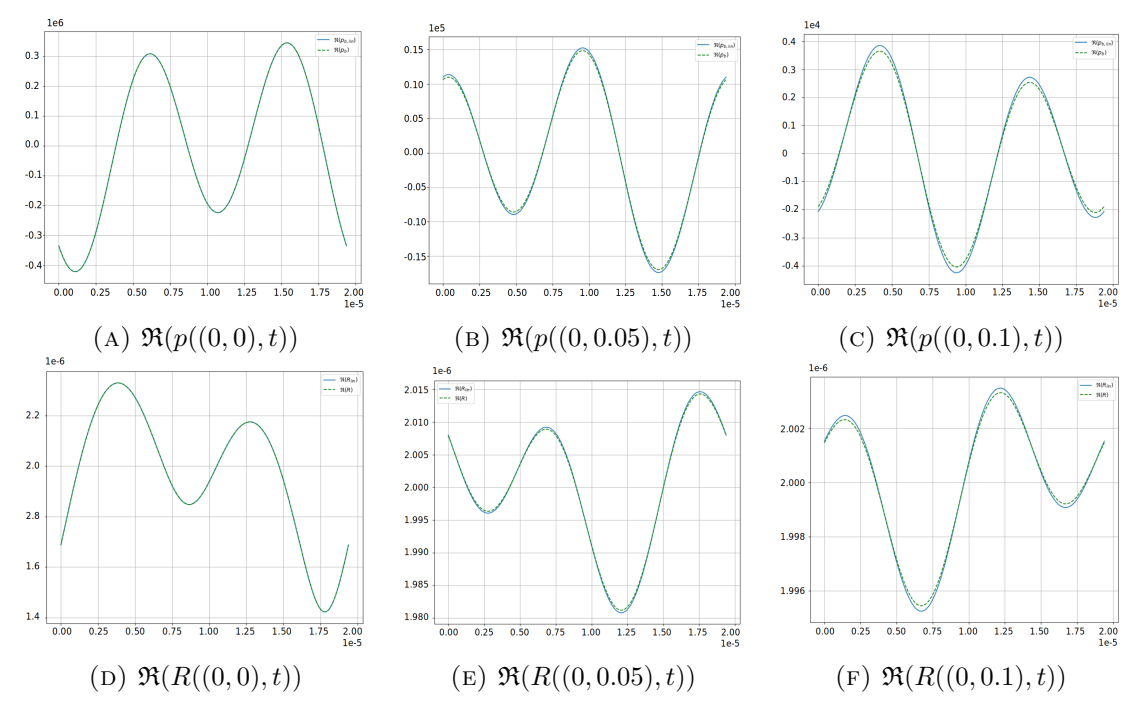


FIGURE 10. Real part of the pressure and radius from the linear (that is, (5.8), blue line) and nonlinear model (that is, (5.7), dashed green line) in terms of pressure over time at three spatial points.

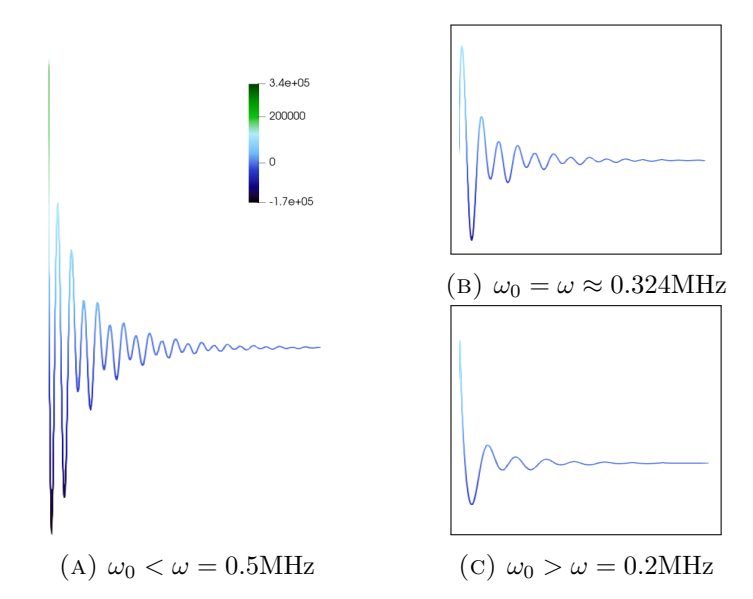


FIGURE 11. Real part of the pressure $\Re(p(x, y_0, t_0))$ obtained from the two-harmonic scheme (5.7) at different driving frequencies ω .

6.5. **Numerical conclusions.** The numerical results demonstrate that microbubbles introduce significant attenuation and phase shifts to the wave propagation, particularly at

greater distances from the source. The impact increases with microbubble density and source amplitude, and is further influenced by the driving frequency.

Concerning the number of harmonics N, in the considered numerical settings using three to five harmonics within the simplified multiharmonic framework obtained from complex fields provides a good compromise between computational efficiency and accuracy. This relatively low number of harmonics makes the approach promising for use in practical applications.

Outlook

In practice, nonlinear acoustic interactions between bubbles and ultrasound waves generate not only harmonics, which are frequency components at integer multiples of the driving frequency, but also subharmonics, which appear at fractional multiples of the driving frequency, such as $\frac{\omega}{2}$, $\frac{\omega}{3}$, ..., see, e.g. [25]. Subharmonics primarily appear due to non-spherical deformations and multibubble interactions. While these effects are not included in our current model, extending the framework to incorporate them would be an interesting direction for future research.

Expanding the present theoretical and numerical framework to explore other phenomena relevant to applications of focused ultrasound waves is also of practical interest. For instance, localized heating, cavitation, and nonlocal attenuation play an important role in therapeutic ultrasound applications such as targeted drug delivery, and it would be worthwhile to investigate the potential role of multiharmonic expansions in these modeling contexts.

Furthermore, investigating inverse problems related to reconstructing spatially varying parameters, such as the bubble number density $n_0 = n_0(x)$ or the nonlinearity parameter $\beta_a = \beta_a(x)$ from measured acoustic signals, is an important task in the context of contrast-enhanced ultrasound imaging, as it could help improve diagnostic accuracy in the long run.

Acknowledgments. We are thankful to Prof. Barbara Kaltenbacher (University of Klagenfurt) for her valuable comments. This research was funded in part by the Austrian Science Fund (FWF) [10.55776/DOC78].

For open-access purposes, the authors have applied a CC BY public copyright license to any author-accepted manuscript version arising from this submission.

Appendices

A. Proof of Lemma 2.1

We present here the postponed proof of Lemma 2.1.

Proof. We can write the linearized second-order ODE in the matrix system form with $V = [v \ v_t]^T$:

(A.1)
$$V_t = AV + F, \quad A = \begin{bmatrix} 0 & 1 \\ -\omega_0^2 & -\delta\omega_0 \end{bmatrix}, \ F = \begin{bmatrix} 0 \\ f \end{bmatrix}$$

a.e. in space. Let $v^{(1)}$ and $v^{(2)}$ be to linearly independent solutions of the homogeneous equation $v_{tt} + \delta \omega_0 v_t + \omega_0^2 v = 0$.

$$(v^{(1)}, v^{(2)}) = \begin{cases} (e^{r_1 t}, e^{r_2 t}), & r_{1,2} = \frac{-\delta \omega_0 \pm \sqrt{\delta^2 \omega_0^2 - 4\omega_0^2}}{2} & \text{if } \delta \omega_0 > 2\omega_0, \\ (e^{-\omega_0 t}, te^{-\omega_0 t}), & \text{if } \delta \omega_0 = 2\omega_0, \\ e^{-\delta \omega_0 t/2}(\cos \alpha t, \sin \alpha t), & \alpha = \frac{\sqrt{4\omega_0^2 - \delta^2 \omega_0^2}}{2} & \text{if } \delta \omega_0 < 2\omega_0. \end{cases}$$

(i) Let first $\delta\omega_0 > 2\omega_0$. Then the fundamental matrix is given by

$$Z(t) = \begin{bmatrix} v^{(1)} & v^{(2)} \\ (v^{(1)})' & (v^{(2)})' \end{bmatrix} = \begin{bmatrix} e^{r_1 t} & e^{r_2 t} \\ r_1 e^{r_1 t} & r_2 e^{r_2 t} \end{bmatrix},$$

and we have

$$(Z(t))^{-1} = \frac{1}{r_2 - r_1} e^{-(r_1 + r_2)t} \begin{bmatrix} r_2 e^{r_2 t} & -e^{r_2 t} \\ -r_1 e^{r_1 t} & e^{r_1 t} \end{bmatrix},$$

where $r_1 - r_2 = \sqrt{\delta^2 \omega_0^2 - 4\omega_0^2}$ and $r_1 + r_2 = -\delta \omega_0$. Then the principal fundamental matrix is

$$\begin{split} X(t) &= Z(t) \left(Z(0) \right)^{-1} = \frac{1}{r_2 - r_1} \begin{bmatrix} e^{r_1 t} & e^{r_2 t} \\ r_1 e^{r_1 t} & r_2 e^{r_2 t} \end{bmatrix} \begin{bmatrix} r_2 & -1 \\ -r_1 & 1 \end{bmatrix} \\ &= \frac{1}{r_2 - r_1} \begin{bmatrix} r_2 e^{r_1 t} - r_1 e^{r_2 t} & -e^{r_1 t} + e^{r_2 t} \\ r_1 r_2 \left(e^{r_1 t} - e^{r_2 t} \right) & -r_1 e^{r_1 t} + r_2 e^{r_2 t} \end{bmatrix}. \end{split}$$

Note that $X_t = AX$. Furthermore,

$$(X(t))^{-1} = \frac{1}{r_2 - r_1} \begin{bmatrix} r_2 e^{-r_1 t} - r_1 e^{-r_2 t} & -e^{-r_1 t} + e^{-r_2 t} \\ r_1 r_2 (e^{-r_1 t} - e^{-r_2 t}) & -r_1 e^{-r_1 t} + r_2 e^{-r_2 t} \end{bmatrix}.$$

Then using the method of variation of parameters, we find that the solution of (A.1) has the form

(A.2)
$$V(t) = X(t) \left(V(0) + \int_0^t (X(\tau))^{-1} f(\tau) d\tau \right).$$

Since periodic solutions must satisfy V(0) = V(T), we then conclude that

$$(I - X(T))V(0) = X(T) \int_0^T (X(\tau))^{-1} f(\tau) d\tau.$$

We have

$$\det(I - X(T)) = 1 - (e^{r_1 T} + e^{r_2 T}) + e^{(r_1 + r_2)T} = (1 - e^{r_1 T})(1 - e^{r_2 T}) \neq 0.$$

Therefore, since the matrix I - X(T) is invertible, we find that

(A.3)
$$V(0) = (I - X(T))^{-1} X(T) \int_0^T (X(\tau))^{-1} f(\tau) d\tau.$$

Furthermore, from (A.2) and (A.3), we have the following bound:

$$||V||_{L^{\infty}(L^{\infty}(\Omega))} + ||V_t||_{L^2(L^{\infty}(\Omega))} \lesssim ||f||_{L^2(L^{\infty}(\Omega))}.$$

(ii) Let next $\delta\omega_0=2\omega_0$. Then the fundamental matrix is given by

$$Z(t) = e^{-\omega_0 t} \begin{bmatrix} 1 & t \\ -\omega_0 & 1 - \omega_0 t \end{bmatrix}, \quad (Z(t))^{-1} = e^{\omega_0 t} \begin{bmatrix} 1 - \omega_0 t & -t \\ \omega_0 & 1 \end{bmatrix}.$$

Then

$$X(t) = e^{-\omega_0 t} \begin{bmatrix} 1 & t \\ -\omega_0 & 1 - \omega_0 t \end{bmatrix} \begin{bmatrix} 1 & 0 \\ \omega_0 & 1 \end{bmatrix} = e^{-\omega_0 t} \begin{bmatrix} 1 + t\omega_0 & t \\ -\omega_0^2 t & 1 - \omega_0 t \end{bmatrix}$$

and

$$(X(t))^{-1} = e^{\omega_0 t} \begin{bmatrix} 1 - \omega_0 t & -t \\ \omega_0^2 t & 1 + \omega_0 t \end{bmatrix}.$$

Then using the method of variation of parameters, we find that the solution has the form

$$V(t) = X(t) \left(V(0) + \int_0^t (X(\tau))^{-1} f(\tau) d\tau \right).$$

Since periodic solutions must satisfy V(0) = V(T), we then have

$$(I - X(T))V(0) = X(T) \int_0^T (X(\tau))^{-1} f(\tau) d\tau$$

and

$$\det(I - X(T)) = (1 - e^{-\omega_0 T})^2 > 0.$$

so we can reason similarly to the first case.

(iii): Lastly, let $\delta \in (0,2)$. The fundamental matrix is then given by

$$Z(t) = e^{-\delta\omega_0 t/2} \begin{bmatrix} \cos\alpha t & \sin\alpha t \\ -\frac{\delta\omega_0}{2}\cos\alpha t - \alpha\sin\alpha t & -\frac{\delta\omega_0}{2}\sin\alpha t + \alpha\cos\alpha t \end{bmatrix}.$$

We have

$$(Z(0))^{-1} = \frac{1}{\alpha} \begin{bmatrix} \alpha & 0 \\ \frac{\delta \omega_0}{2} & 1 \end{bmatrix}.$$

Let $X(t) = Z(t)(Z(0))^{-1}$, we have

$$X(t) = \frac{1}{\alpha} e^{-\delta\omega_0 t/2} \begin{bmatrix} \cos\alpha t & \sin\alpha t \\ -\frac{\delta\omega_0}{2}\cos\alpha t - \alpha\sin\alpha t & -\frac{\delta\omega_0}{2}\sin\alpha t + \alpha\cos\alpha t \end{bmatrix} \begin{bmatrix} \alpha & 0 \\ \frac{\delta\omega_0}{2} & 1 \end{bmatrix}$$
$$= \frac{1}{\alpha} e^{-\delta\omega_0 t/2} \begin{bmatrix} \alpha\cos\alpha t + \frac{\delta\omega_0}{2}\sin\alpha t & \sin\alpha t \\ (-\alpha^2 - \frac{\delta^2\omega_0^2}{4})\sin\alpha t & \alpha\cos\alpha t - \frac{\delta\omega_0}{2}\sin\alpha t \end{bmatrix}$$

and

$$(X(t))^{-1} = \frac{1}{\alpha} e^{\delta\omega_0 t/2} \begin{bmatrix} \alpha \cos \alpha t - \frac{\delta\omega_0}{2} \sin \alpha t & -\sin \alpha t \\ (\alpha^2 + \frac{\delta^2\omega_0^2}{4}) \sin \alpha t & \alpha \cos \alpha t + \frac{\delta\omega_0}{2} \sin \alpha t \end{bmatrix}.$$

Then again using the method of variation of parameters, we find that the solution has the form

$$V(t) = X(t) \left(V(0) + \int_0^t (X(\tau))^{-1} f(\tau) d\tau \right),$$

and

$$\det(I - X(T)) = 1 + e^{-T\delta\omega_0} - 2e^{-T\frac{\delta\omega_0}{2}}\cos\alpha T = (e^{-T\frac{\delta\omega_0}{2}} - \cos\alpha T)^2 + \sin^2\alpha T > 0$$

since $\delta > 0$. Since periodic solutions must satisfy V(0) = V(T), we then have

$$V(0) = (I - X(T))^{-1} X(T) \int_0^T (X(\tau))^{-1} f(\tau) d\tau,$$

and arrive at the desired estimate in the same manner as before.

B. Proof of the cut-off error estimate (4.2)

We provide here the proof of the error estimate

for $(p,v) \in (Y_p^\ell \cap H^{\ell+2}(0,T;H^1(\Omega))) \times Y_v^\ell$, which follows by a straightforward modification of the arguments in [3, Lemma 12].

proof of (4.2). We can express the norms as follows:

$$\begin{split} \|p\|_{Y_p^0\cap H^2(H^1(\Omega))}^2 &= \int_0^T \left(\|\nabla p\|_{L^2(\Omega)}^2 + \|\nabla p_t\|_{L^2(\Omega)}^2 + \|\nabla p_{tt}\|_{L^2(\Omega)}^2 \right. \\ &\quad + \|p\|_{L^2(\Omega)}^2 + \|p_t\|_{L^2(\Omega)}^2 + \|p_{tt}\|_{L^2(\Omega)}^2 \\ &\quad + \|p\|_{L^2(\partial\Omega)}^2 + \|p_t\|_{L^2(\partial\Omega)}^2 + \|p_{tt}\|_{L^2(\partial\Omega)}^2 \right) \mathrm{d}t \\ &= \frac{T}{2} \sum_{m=0}^\infty \left\{ \left(1 + (m\omega)^2 + (m\omega)^4 \right) \left(\|\nabla p_m^c\|_{L^2(\Omega)}^2 + \|\nabla p_m^s\|_{L^2(\Omega)}^2 \right) \right. \\ &\quad + \left. \left(1 + (m\omega)^2 + (m\omega)^4 \right) \left(\|p_m^c\|_{L^2(\Omega)}^2 + \|p_m^s\|_{L^2(\Omega)}^2 \right) \right. \\ &\quad + \left. \left(1 + (m\omega)^2 + (m\omega)^4 \right) \left(\|p_m^c\|_{L^2(\partial\Omega)}^2 + \|p_m^s\|_{L^2(\partial\Omega)}^2 \right) \right\} \end{split}$$

and, similarly,

$$||v||_{Y_v^0}^2 = \frac{T}{2} \sum_{m=0}^{\infty} \left\{ \left(1 + (m\omega)^2 + (m\omega)^4 \right) \left(||v_m^c||_{L^2(\Omega)}^2 + ||v_m^s||_{L^2(\Omega)}^2 \right) \right\}.$$

Therefore, the errors are given by

$$\begin{split} \|p - \tilde{p}^N\|_{Y_p^0 \cap H^2(H^1(\Omega))}^2 &= \frac{T}{2} \sum_{m=N+1}^{\infty} \left\{ \left(1 + (m\omega)^2 + (m\omega)^4 \right) \left(\|\nabla p_m^c\|_{L^2(\Omega)}^2 + \|\nabla p_m^s\|_{L^2(\Omega)}^2 \right) \right. \\ &\quad + \left(1 + (m\omega)^2 + (m\omega)^4 \right) \left(\|p_m^c\|_{L^2(\Omega)}^2 + \|p_m^s\|_{L^2(\Omega)}^2 \right) \\ &\quad + \left(1 + (m\omega)^2 + (m\omega)^4 \right) \left(\|p_m^c\|_{L^2(\partial\Omega)}^2 + \|p_m^s\|_{L^2(\partial\Omega)}^2 \right) \right\} \end{split}$$

and

$$\|v - \tilde{v}^N\|_{Y_v^0}^2 = \frac{T}{2} \sum_{m=N+1}^{\infty} \left\{ \left(1 + (m\omega)^2 + (m\omega)^4\right) \left(\|v_m^c\|_{L^2(\Omega)}^2 + \|v_m^s\|_{L^2(\Omega)}^2\right) \right\}.$$

We then have the estimate

$$\begin{split} &\|p - \tilde{p}^N\|_{Y_p^0 \cap H^2(H^1(\Omega))}^2 \\ &\leq \frac{T}{2} \tilde{C} \max_{m \geq N+1} \frac{1}{1 + (m\omega)^{2\ell}} \sum_{m=N+1}^{\infty} \Big\{ \Big(1 + (m\omega)^2 + \ldots + (m\omega)^{2\ell+4} \Big) \, \Big(\|\nabla p_m^c\|_{L^2(\Omega)}^2 + \|\nabla p_m^s\|_{L^2(\Omega)}^2 \Big) \\ &\quad + \Big(1 + (m\omega)^2 + (m\omega)^4 + \ldots + (m\omega)^{2\ell+4} \Big) \, \Big(\|p_m^c\|_{L^2(\Omega)}^2 + \|p_m^s\|_{L^2(\Omega)}^2 \Big) \\ &\quad + \Big(1 + (m\omega)^2 + (m\omega)^4 + \ldots + (m\omega)^{2\ell+4} \Big) \, \Big(\|p_m^c\|_{L^2(\partial\Omega)}^2 + \|p_m^s\|_{L^2(\partial\Omega)}^2 \Big) \Big\} \Big\}. \end{split}$$

for some $\tilde{C} > 0$, independent of N. From here, we conclude that

$$||p - \tilde{p}^N||_{Y_p^0 \cap H^2(H^1(\Omega))}^2 \le \frac{T}{2} \tilde{C} \frac{1}{1 + ((N+1)\omega)^{2\ell}} ||p||_{Y_p^\ell \cap H^{\ell+2}(H^1(\Omega))}^2$$
$$\le CN^{-2\ell} ||p||_{Y_p^\ell \cap H^{\ell+2}(H^1(\Omega))}^2.$$

for some C > 0, independent of N. We can analogously derive the estimate

$$||v - \tilde{v}^N||_{Y_p^0}^2 \le \tilde{C}N^{-2\ell}||v||_{Y_v^\ell}^2,$$

to conclude the proof.

C. Proof of estimate (4.5)

We provide here the proof of (4.5). We start from

(C.1)
$$\langle \mathcal{L}_1 e^{p,N}, \phi^N \rangle = -\int_0^T \int_{\Omega} f^N \phi^N \, \mathrm{d}x \mathrm{d}s + \langle \mathcal{L}_1 \mathrm{err}(\tilde{p}^N), \phi^N \rangle$$

with the short-hand notation

$$f^{N} = (p^{2} - (p^{N-1})^{2})_{tt} + c^{2}\rho_{0}n_{0}(v_{tt} - v_{tt}^{N}).$$

The proof follows by testing (C.1) with $e^{p,N}$, $e^{p,N}_t$, and $e^{p,N}_{tt}$ and exploiting the time-periodic conditions.

Step I: Testing (C.1) with $e^{p,N}$ leads to

$$c^{2} \|\nabla e^{p,N}\|_{L^{2}(L^{2}(\Omega))}^{2} + c^{2} \gamma \|e^{p,N}\|_{L^{2}(L^{2}(\partial\Omega))}^{2}$$

$$= -\int_{0}^{T} \int_{\Omega} e_{tt}^{p,N} e^{p,N} \, \mathrm{d}x \mathrm{d}s - \int_{0}^{T} \int_{\partial\Omega} b \beta e_{tt}^{p,N} e^{p,N} \, \mathrm{d}\Gamma \mathrm{d}s$$

$$-\int_{0}^{T} \int_{\Omega} f^{N} e^{p,N} \, \mathrm{d}x \mathrm{d}s + \langle \mathcal{L}_{1} \mathrm{err}(\tilde{p}^{N}), e^{p,N} \rangle.$$

Above, we have relied on the fact that

$$\int_0^T \int_{\Omega} b \nabla e_t^{p,N} \cdot \nabla e^{p,N} \, \mathrm{d}x \mathrm{d}s = 0 \quad \text{and} \quad \int_0^T \int_{\partial \Omega} (c^2 \beta + b \gamma) e_t^{p,N} e^{p,N} \, \mathrm{d}\Gamma \mathrm{d}s = 0$$

due to time-periodic conditions. We can further use integration by parts in time together with $e^{p,N}(0)=e^{p,N}(T)$ and $e^{p,N}_t(0)=e^{p,N}_t(T)$ to conclude that

$$-\int_{0}^{T} \int_{\Omega} e_{tt}^{p,N} e^{p,N} \, \mathrm{d}x \mathrm{d}s - \int_{0}^{T} \int_{\partial \Omega} b\beta e_{tt}^{p,N} e^{p,N} \, \mathrm{d}\Gamma \mathrm{d}s$$
$$= \|e_{t}^{p,N}\|_{L^{2}(L^{2}(\Omega))}^{2} + b\beta \|e_{t}^{p,N}\|_{L^{2}(L^{2}(\Omega))}^{2}.$$

Furthermore, we have

$$< \mathcal{L}_{1}\mathrm{err}(\tilde{p}^{N}), e^{p,N} >$$

$$:= \int_{0}^{T} \int_{\Omega} \left((\mathrm{err}(\tilde{p}^{N}))_{tt} e^{p,N} + c^{2} \nabla \mathrm{err}(\tilde{p}^{N}) \cdot \nabla e^{p,N} + b \nabla (\mathrm{err}(\tilde{p}^{N}))_{t} \cdot \nabla e^{p,N} \right) \, \mathrm{d}x \mathrm{d}s$$

$$+ \int_{0}^{T} \int_{\partial \Omega} (c^{2} (\beta (\mathrm{err}(\tilde{p}^{N}))_{t} + \gamma \mathrm{err}(\tilde{p}^{N})) + b (\beta (\mathrm{err}(\tilde{p}^{N}))_{tt} + \gamma (\mathrm{err}(\tilde{p}^{N}))_{t})) e^{p,N} \, \mathrm{d}\Gamma \mathrm{d}s.$$

and thus using Hölder's and Young's inequalities leads to

$$\begin{aligned} & \left| < \mathcal{L}_{1}\mathrm{err}(\tilde{p}^{N}), e^{p,N} > \right| \\ & \lesssim \varepsilon \|e^{p,N}\|_{L^{2}(L^{2}(\Omega))}^{2} + \varepsilon \|\nabla e^{p,N}\|_{L^{2}(L^{2}(\Omega))}^{2} + \varepsilon \|\nabla e^{p,N}\|_{L^{2}(L^{2}(\Omega))}^{2} + \varepsilon \|e^{p,N}\|_{L^{2}(L^{2}(\partial\Omega))}^{2} \\ & + \|(\mathrm{err}(\tilde{p}^{N}))_{tt}\|_{L^{2}(L^{2}(\Omega))}^{2} + \|\nabla \mathrm{err}(\tilde{p}^{N})\|_{H^{1}(L^{2}(\Omega))}^{2} + \|\mathrm{err}(\tilde{p}^{N})\|_{H^{2}(L^{2}(\partial\Omega))}^{2} \end{aligned}$$

for any $\varepsilon > 0$. Similarly,

$$\left| - \int_0^T \int_{\Omega} f^N e^{p,N} \, \mathrm{d}x \, \mathrm{d}s \right| \lesssim \|f^N\|_{L^2(L^2(\Omega))}^2 + \varepsilon \|e^{p,N}\|_{L^2(L^2(\Omega))}^2.$$

Thus, for ε sufficiently small, the outcome of testing in Step I can be formulated as

$$\begin{split} \|\nabla e^{p,N}\|_{L^2(L^2(\Omega))}^2 + \|e^{p,N}\|_{L^2(L^2(\partial\Omega))}^2 \lesssim \varepsilon \|e^{p,N}\|_{L^2(L^2(\Omega))}^2 + \varepsilon \|\nabla e_t^{p,N}\|_{L^2(L^2(\Omega))}^2 \\ + \|f^N\|_{L^2(L^2(\Omega))}^2 + \|\operatorname{err}(\tilde{p}^N)\|_{Y_p^0}^2. \end{split}$$

Further using the equivalence of $\|\nabla w\|_{L^2(\Omega)}^2 + \|w\|_{L^2(\partial\Omega)}^2$ and $\|w\|_{H^1(\Omega)}^2$ yields for small ε

$$\|e^{p,N}\|_{L^2(H^1(\Omega))}^2 \lesssim \varepsilon \|\nabla e_t^{p,N}\|_{L^2(L^2(\Omega))}^2 + \|f^N\|_{L^2(L^2(\Omega))}^2 + \|\mathrm{err}(\tilde{p}^N)\|_{Y_p^0}^2.$$

Step II: Testing (C.1) with $e_t^{p,N}$ and exploiting time-periodicity leads to

$$b\|\nabla e_t^{p,N}\|_{L^2(L^2(\Omega))}^2 + (c^2 + \gamma)\beta\|e_t^{p,N}\|_{L^2(L^2(\partial\Omega))}^2$$

= $-\int_0^T \int_{\Omega} f^N e_t^{p,N} dxds + \langle \mathcal{L}_1 \text{err}(\tilde{p}^N), e_t^{p,N} \rangle.$

Then proceeding similarly to Step I results in

$$\|e_t^{p,N}\|_{L^2(H^1(\Omega))}^2 \lesssim \|f^N\|_{L^2(L^2(\Omega))}^2 + \|\mathrm{err}(\tilde{p}^N)\|_{Y_p^0}^2.$$

Step III: Testing (C.1) with $e_{tt}^{p,N}$ and exploiting time-periodicity leads to

$$b\|e_{tt}^{p,N}\|_{L^{2}(L^{2}(\Omega))}^{2} + b\beta\|e_{tt}^{p,N}\|_{L^{2}(L^{2}(\partial\Omega))}^{2}$$

$$= -c^{2} \int_{0}^{T} \int_{\Omega} \nabla e^{p,N} \cdot \nabla e_{tt}^{p,N} - c^{2} \gamma \int_{0}^{T} \int_{\partial\Omega} e^{p,N} e_{tt}^{p,N} d\Gamma ds$$

$$- \int_{0}^{T} \int_{\Omega} f^{N} e_{tt}^{p,N} dx ds + \langle \mathcal{L}_{1} \text{err}(\tilde{p}^{N}), e_{tt}^{p,N} \rangle.$$

By time-periodicity, we have

$$\begin{split} &-c^2 \int_0^T \int_{\Omega} \nabla e^{p,N} \cdot \nabla e_{tt}^{p,N} - c^2 \gamma \int_0^T \int_{\partial \Omega} e^{p,N} e_{tt}^{p,N} \, \mathrm{d}\Gamma \mathrm{d}s \\ &= c^2 \|\nabla e_t^{p,N}\|_{L^2(L^2(\Omega))}^2 + c^2 \gamma \|e_t^{p,N}\|_{L^2(L^2(\partial \Omega))}^2. \end{split}$$

Furthermore, we have

$$<\mathcal{L}_{1}\mathrm{err}(\tilde{p}^{N}), e_{tt}^{p,N}>$$

$$:= \int_{0}^{T} \int_{\Omega} \left((\mathrm{err}(\tilde{p}^{N}))_{tt} e_{tt}^{p,N} + c^{2} \nabla \mathrm{err}(\tilde{p}^{N}) \cdot \nabla e_{tt}^{p,N} + b \nabla (\mathrm{err}(\tilde{p}^{N}))_{t} \cdot \nabla e_{tt}^{p,N} \right) dxds$$

$$+ \int_{0}^{T} \int_{\partial \Omega} (c^{2} (\beta (\mathrm{err}(\tilde{p}^{N}))_{t} + \gamma \mathrm{err}(\tilde{p}^{N})) + b (\beta (\mathrm{err}(\tilde{p}^{N}))_{tt} + \gamma (\mathrm{err}(\tilde{p}^{N}))_{t})) e_{tt}^{p,N} d\Gamma ds.$$

We integrate by parts in time in the c^2 and b terms on the left-hand side:

$$\int_{0}^{T} \int_{\Omega} \left(c^{2} \nabla \operatorname{err}(\tilde{p}^{N}) \cdot \nabla e_{tt}^{p,N} + b \nabla (\operatorname{err}(\tilde{p}^{N}))_{t} \cdot \nabla e_{tt}^{p,N} \right) dx ds$$

$$= - \int_{0}^{T} \int_{\Omega} \left(c^{2} \nabla (\operatorname{err}(\tilde{p}^{N}))_{t} \cdot \nabla e_{t}^{p,N} + b \nabla (\operatorname{err}(\tilde{p}^{N}))_{tt} \cdot \nabla e_{t}^{p,N} \right) dx ds$$

and then estimate

$$\left| \langle \mathcal{L}_{1} \mathrm{err}(\tilde{p}^{N}), e_{tt}^{p,N} \rangle \right| \lesssim \varepsilon \|e_{tt}^{p,N}\|_{L^{2}(L^{2}(\Omega))}^{2} + \varepsilon \|\nabla e_{t}^{p,N}\|_{L^{2}(\Omega)}^{2} + \varepsilon \|e_{tt}^{p,N}\|_{L^{2}(L^{2}(\partial\Omega))}^{2}
+ \|(\mathrm{err}(\tilde{p}^{N}))_{tt}\|_{L^{2}(L^{2}(\Omega))}^{2} + \|\nabla(\mathrm{err}(\tilde{p}^{N}))_{t}\|_{L^{2}(L^{2}(\Omega))}^{2}
+ \|\nabla(\mathrm{err}(\tilde{p}^{N}))_{tt}\|_{L^{2}(L^{2}(\Omega))}^{2} + \|\mathrm{err}(\tilde{p}^{N})\|_{H^{2}(\partial\Omega)}^{2}.$$

Note that the presence of the term $\|\nabla(\operatorname{err}(\tilde{p}^N))_{tt}\|_{L^2(L^2(\Omega))}^2$ above is the reason for needing $p \in H^{\ell+2}(0,T;H^1(\Omega))$ (in addition to $p \in \mathcal{X}_p \cap Y_p^{\ell}$). We also have

$$\left| - \int_0^T \int_{\Omega} f^N e_{tt}^{p,N} \, \mathrm{d}x \, \mathrm{d}s \right| \lesssim \|f^N\|_{L^2(L^2(\Omega))}^2 + \varepsilon \|e_{tt}^{p,N}\|_{L^2(L^2(\Omega))}^2.$$

Thus, the outcome of testing in Step III for small enough ε is

$$||e_{tt}^{p,N}||_{L^{2}(L^{2}(\Omega))}^{2} + ||e_{tt}^{p,N}||_{L^{2}(L^{2}(\partial\Omega))}^{2}$$

$$\leq \varepsilon ||\nabla e_{t}^{p,N}||_{L^{2}(\Omega)}^{2} + ||f^{N}||_{L^{2}(L^{2}(\Omega))}^{2} + ||\operatorname{err}(\tilde{p}^{N})||_{Y_{p}^{0} \cap H^{2}(H^{1}(\Omega))}^{2}.$$

Combining the three obtained estimates leads to (4.5) provided ε is sufficiently small.

References

- [1] S. Acosta, G. Uhlmann, and J. Zhai, Nonlinear ultrasound imaging modeled by a Westervelt equation, SIAM Journal on Applied Mathematics, 82 (2022), pp. 408–426.
- [2] I. Babuška and S. Sauter, Is the pollution effect of the FEM avoidable for the Helmholtz equation considering high wavenumber?, SIAM Review, 42 (2000), pp. 451–484.
- [3] F. Bachinger, U. Langer, and J. Schöberl, Numerical analysis of nonlinear multiharmonic eddy current problems, Numerische Mathematik, 100 (2005), pp. 593–616.
- [4] —, Efficient solvers for nonlinear time-periodic eddy current problems, Computing and Visualization in Science, 9 (2006), pp. 197–207.
- [5] I. A. BARATTA, J. P. DEAN, J. S. DOKKEN, M. HABERA, J. S. HALE, C. N. RICHARDSON, M. E. ROGNES, M. W. SCROGGS, N. SIME, AND G. N. WELLS, DOLFINx: The next generation FEniCS problem solving environment, Dec. 2023.
- [6] N. BLANKEN, B. HEILES, A. KULIESH, M. VERSUIS, K. JAIN, D. MARESCA, AND G. LAJOINIE, *PROTEUS: A physically realistic contrast-enhanced ultrasound simulator—Part I: Numerical methods*, IEEE Transactions on Ultrasonics, Ferroelectrics, and Frequency Control, (2024).
- [7] A. CELIK AND M. KYED, Nonlinear wave equation with damping: Periodic forcing and non-resonant solutions to the Kuznetsov equation, ZAMM-Journal of Applied Mathematics and Mechanics/Zeitschrift für Angewandte Mathematik und Mechanik, 98 (2018), pp. 412–430.
- [8] —, Nonlinear acoustics: Blackstock-Crighton equations with a periodic forcing term, Journal of Mathematical Fluid Mechanics, 21 (2019), pp. 1–12.
- [9] H. DE GERSEM, H. VANDE SANDE, AND K. HAMEYER, Strong coupled multiharmonic finite element simulation package, COMPEL-The international journal for computation and mathematics in electrical and electronic engineering, 20 (2001), pp. 535–546.
- [10] A. A. Doinikov and A. Bouakaz, Review of shell models for contrast agent microbubbles, IEEE transactions on ultrasonics, ferroelectrics, and frequency control, 58 (2011), pp. 981–993.
- [11] N. EPTAMINITAKIS AND P. STEFANOV, Weakly nonlinear geometric optics for the Westervelt equation and recovery of the nonlinearity, SIAM Journal on Mathematical Analysis, 56 (2024), pp. 801–819.
- [12] K. Ferrara, R. Pollard, and M. Borden, *Ultrasound microbubble contrast agents: fundamentals and application to gene and drug delivery*, Annu. Rev. Biomed. Eng., 9 (2007), pp. 415–447.
- [13] C. GEUZAINE AND J.-F. REMACLE, Gmsh: A 3-d finite element mesh generator with built-in pre- and post-processing facilities, International Journal for Numerical Methods in Engineering, 79 (2009), pp. 1309 1331.
- [14] R. Grimshaw, Nonlinear ordinary differential equations, Routledge, 2017.
- [15] R. Hakl and M. Zamora, Periodic solutions to the Liénard type equations with phase attractive singularities, Boundary Value Problems, 2013 (2013), pp. 1–20.
- [16] M. F. Hamilton and D. T. Blackstock, *Nonlinear acoustics*, vol. 237, Academic press San Diego, 1998.

- [17] L. Hoff, Acoustic characterization of contrast agents for medical ultrasound imaging, Springer Science & Business Media, 2001.
- [18] F. IHLENBURG AND I. BABUŠKA, Finite element solution of the helmholtz equation with high wave number Part I: The h-version of the FEM, Computers & Mathematics with Applications, 30 (1995), pp. 9–37.
- [19] B. Kaltenbacher, *Mathematics of nonlinear acoustics*, Evolution Equations and Control Theory, 4 (2015), pp. 447–491.
- [20] —, Periodic solutions and multiharmonic expansions for the Westervelt equation., Evolution Equations & Control Theory, 10 (2021).
- [21] —, Well-posedness of the time-periodic Jordan-Moore-Gibson-Thompson equation, arXiv preprint arXiv:2409.05355, (2024).
- [22] —, Acoustic nonlinearity parameter tomography with the Jordan-Moore-Gibson-Thompson equation in frequency domain, arXiv preprint arXiv:2502.05810, (2025).
- [23] B. Kaltenbacher and I. Lasiecka, Global existence and exponential decay rates for the Westervelt equation, Discrete & Continuous Dynamical Systems-S, 2 (2009), p. 503.
- [24] B. Kaltenbacher and W. Rundell, On the identification of the nonlinearity parameter in the Westervelt equation from boundary measurements, Inverse Problems and Imaging, 15 (2021), pp. 865–891.
- [25] P. Krishna, P. Shankar, and V. Newhouse, Subharmonic generation from ultrasonic contrast agents, Physics in medicine & biology, 44 (1999), p. 681.
- [26] J. Lu, X. Zhao, and S. Yamada, Introduction to Harmonic Balance Finite Element Method (HBFEM), 2016, pp. 1–18.
- [27] A. MATALLIOTAKIS AND M. VERWEIJ, Computation of ultrasound propagation in a population of nonlinearly oscillating microbubbles including multiple scattering, The Journal of the Acoustical Society of America, 153 (2023), pp. 2209–2209.
- [28] J. MELENK AND S. SAUTER, Convergence analysis for finite element discretizations of the Helmholtz equation with Dirichlet-to-Neumann boundary conditions, Math. Comput., 79 (2010).
- [29] J. Nečas, Direct methods in the theory of elliptic equations, Springer Science & Business Media, 2011.
- [30] V. Nikolić and T. Rauscher, Mathematical models for nonlinear ultrasound contrast imaging with microbubbles, SIAM Journal on Applied Mathematics, (to appear).
- [31] B. RAINER AND B. KALTENBACHER, Existence, uniqueness, and numerical solutions of the nonlinear periodic Westervelt equation, arXiv preprint arXiv:2407.17043v4, (2024).
- [32] G. Schmidt, Yakubovich, V. A./Starzhinskii, V. M., Linear Differential Equations with Periodic Coefficients, Vol. 1 und 2, Übersetzung aus dem Russischen, 839 S., 1975. John-Wiley & Sons New York-Toronto, Israel Program for Scientific Translations, Serusalem-London., ZAMM Journal of Applied Mathematics and Mechanics/ Zeitschrift für Angewandte Mathematik und Mechanik, 56 (1976), pp. 222–222.
- [33] E. Stride, Physical principles of microbubbles for ultrasound imaging and therapy, Cerebrovascular Diseases, 27 (2009).
- [34] P. J. TORRES, Mathematical models with singularities, vol. 1, Springer, 2015.
- [35] P. L. M. J. VAN NEER, M. G. DANILOUCHKINE, M. D. VERWEIJ, L. DEMI, M. M. VOORMOLEN, A. F. W. VAN DER STEEN, AND N. DE JONG, *Comparison*

- of fundamental, second harmonic, and superharmonic imaging: A simulation study, The Journal of the Acoustical Society of America, 130 (2011), pp. 3148–3157.
- [36] M. Versluis, E. Stride, G. Lajoinie, B. Dollet, and T. Segers, *Ultrasound contrast agent modeling: a review*, Ultrasound in medicine & biology, 46 (2020), pp. 2117–2144.
- [37] P. J. WESTERVELT, *Parametric acoustic array*, The Journal of the Acoustical Society of America, 35 (1963), pp. 535–537.
- [38] S. Yamada and K. Bessho, Harmonic field calculation by the combination of finite element analysis and harmonic balance method, IEEE Transactions on Magnetics, 24 (1988), pp. 2588–2590.
- [39] X. Yu, Q. Yuan, and Z. Cheng, Bifurcation and dynamics of periodic solutions to the Rayleigh-Plesset equation: Theory and numerical simulation, Physica D: Nonlinear Phenomena, 459 (2024), p. 134045.